Intestinal alteration of α-gustducin and sweet taste signaling pathway in metabolic diseases is partly rescued after weight loss and diabetes remission Running Head: Intestinal α-gustducin in metabolic diseases

Léa Le Gléau, Christine Rouault, Céline Osinski, Edi Prifti, Hédi Antoine Soula, Jean Debédat, Pauline Busieau, Chloé Amouyal, Karine Clément, Fabrizio Andreelli, et al.

Intestinal alteration of α-gustducin and sweet taste signaling pathway in metabolic diseases is partly rescued after weight loss and diabetes remission

Running Head: Intestinal α-gustducin in metabolic diseases

Léa Le Gléau[1], Christine Rouault[1], Céline Osinski[1], Edi Prifti[1,2], Hédi Antoine Soula[1], Jean Debédat[1], Pauline Busieau[1], Chloé Amouyal[1,3,4], Karine Clément[1,3], Fabrizio Andreelli[1,3,4], Agnès Ribeiro[1]* and Patricia Serradas[1]*

1- Sorbonne Université, INSERM, Nutrition and obesities: systemic approaches (NutriOmics), F-75013 Paris, France

2- IRD, Sorbonne University, UMMISCO, 32 Avenue Henri Varagnat, F-93143 Bondy, France

3- Assistance Publique/Hôpitaux de Paris, APHP, Nutrition department, Pitié-Salpêtrière hospital, Paris F-75013

4- Assistance Publique-Hôpitaux de Paris, APHP, Diabetology-Metabolisms Department, Pitié-Salpêtrière Hospital, Paris F-75013, France.

* Co-Corresponding authors and contributed equally to this work:

Dr. Agnès Ribeiro : agnes.ribeiro@sorbonne-universite.fr / ORCID ID: 0000-0003-2063-6084

Sorbonne Université / INSERM UMR_S 1269

Prof. Patricia Serradas : patricia.serradas_pacheco@sorbonne-universite.fr / ORCID ID: 0000-0002-6652-9746

NutriOmics - Nutrition and obesities: systemic approaches

Faculté de Médecine

91 Bd de l'Hôpital, 6ème étage

75013 Paris FRANCE

Word count: 5303

Abstract

Carbohydrates and sweeteners are detected by the sweet taste receptor in enteroendocrine cells (EEC). This receptor is coupled to the gustducin G-protein, which α-subunit is encoded by *GNAT3* gene. In intestine, the activation of sweet taste receptor triggers a signaling pathway leading to GLP-1 secretion, an incretin hormone. In metabolic diseases GLP-1 concentration and incretin effect are reduced while partly restored after Roux-en-Y gastric bypass (RYGB). We wondered if the decreased GLP-1 secretion in metabolic diseases is caused by an intestinal defect in sweet taste transduction pathway. In our RNA-sequencing of EEC *GNAT3* expression is decreased in patients with obesity and type 2 diabetes compared to normoglycemic obese patients. This prompted us to explore sweet taste signaling pathway in mice with metabolic deteriorations. During obesity onset in mice *Gnat3* expression was downregulated in EEC. After metabolic improvement with entero-gastro anastomosis surgery in mice (a surrogate of the RYGB in humans), the expression of *Gnat3* increased in the new alimentary tract and glucose-induced GLP-1 secretion was improved. In order to evaluate if high-fat diet-induced dysbiotic intestinal microbiota could explain the changes in the expression of sweet taste α-subunit G protein, we performed a fecal microbiota transfer in mice. However, we could not conclude if dysbiotic microbiota impacted or not intestinal *Gnat3* expression. Our data highlight that metabolic disorders were associated with altered gene expression of sweet taste signaling in intestine. This could contribute to impaired GLP-1 secretion that is partly rescued after metabolic improvement.

Key words: Intestinal endocrine cells, α-gustducin, obesity, type 2 diabetes, microbiota

New & Noteworthy

Our data highlighted: 1/ the sweet taste transduction pathway in EECs plays pivotal role for glucose homeostasis at least at gene expression level; 2/ metabolic disorders led to altered gene expression of sweet taste signaling pathway in intestine contributing to

impaired GLP-1 secretion; 3/ after surgical intestinal modifications, increased expression of alpha-gustducin contributed to metabolic improvement.

Abbreviations

CD: control diet; EEC: enteroendocrine cell; EGA: entero-gastro anastomosis; FMT: fecal microbiota transfer; GLP-1: glucagon-like peptide-1; HFD: high-fat diet; HFD-HF: high-fat diet-high fructose; HOMA-IR: Homeostasis Assessment of insulin resistance; PYY: peptide YY; PLCβ2: phospholipase C β2; RYGB: Roux-en-Y gastric bypass; T1R2-T1R3: sweet taste receptor; T2D: Type 2 diabetes

INTRODUCTION

Glucagon Like-Peptide-1 (GLP-1) is an incretin hormone secreted from specialized L-enteroendocrine cells (EECs) which enhances glucose-dependent insulin secretion by two-fold in the postprandial state. The mechanisms by which EEC link glucose detection to GLP-1 secretion is still debated but they involve both sugar transporters and sweet taste receptor (32). This heterodimeric T1R2-T1R3 receptor encoded by *TAS1R2* and *TAS1R3* is coupled to the taste G-protein gustducin composed of α, β and γ subunits encoded respectively by *GNAT3*, *GNB3* and *GNG13* genes (34). Several lines of evidence support that T1R2-T1R3 and α-gustducin are required for glucose-stimulated GLP-1 secretion. Indeed, these three proteins are present in human and rodent L-cells of the small intestine (16, 36, 39). Furthermore, GLP-1 secretion can be elicited from mouse intestinal explants, and/or mouse (GLUTag) and human (NCI-H716) EEC lines by sweet taste receptor agonists — sucrose, glucose, fructose and sucralose (12, 16, 24). Moreover, glucose-stimulated GLP-1 secretion is nearly or fully abolished in α-gustducin$^{-/-}$, TAS1R2$^{-/-}$ and TAS1R3$^{-/-}$ mice (12, 16, 19). This is also the case, when sweet taste receptor are inhibited or silenced using RNA of α-gustducin on GLUTag and NCI-H716 cells (16, 24). Finally, the sweet taste receptor inhibitor, lactisole, reduces circulating levels of GLP-1 and PYY after intragastric or intraduodenal

85 administration of glucose in humans (13, 39). In EECs, the detection of carbohydrates and
86 sweeteners by the sweet taste receptor and the activation of α-gustducin stimulate
87 phospholipase C β2 (PLCβ2),-produce inositol-trisphosphate (IP3), and increase intracellular
88 calcium concentration leading to GLP-1 release. Sodium (TRPM5 and SCN2A) and calcium
89 (CACNA1A) channels are also involved in this signaling pathway (10).
90 The incretin effect seems to be impaired in individuals with type 2 diabetes (T2D) owing to
91 the combined effects of reduced GLP-1 secretion and impaired GIP action (25, 28). Gastric
92 bypass surgery is an effective tool in reducing body weight in individuals with severe obesity
93 (26) and results in the improvement or even complete remission of T2D (9). The rise of post-
94 prandial GLP-1 secretion after Roux-en-Y gastric bypass (RYGB) may contribute to this
95 improvement (7, 14, 23, 33, 43). After RYGB the rapid delivery of undigested nutrients to the
96 lower small intestine may affect the regulation of taste receptors and/or glucose transporters
97 on EECs, resulting in an enhanced release of GLP-1 (2, 20, 45) although a recent study
98 demonstrated that lengthening of the intestinal bypass in RYGB does not affect GLP-1
99 secretion (27). Therefore, the mechanisms driving the alteration of enterohormone secretion
100 in obesity and after RYGB might not be restricted to GLP-1 incretin effects alone (23). Gut
101 microbiota, participates in environmental cues that affect EEC and is altered in metabolic
102 diseases (31). RYGB improves microbiota dysbiosis, although most patients remain with low
103 microbial gene richness despite major metabolic improvement and weight loss (4).
104 We have previously shown a positive association between jejunal GLP-1 cell density and fat-
105 consumption in individuals with severe obesity (3). Moreover, we showed that T2D is
106 associated with impaired jejunal enteroendocrine GLP-1 cell lineage in human obesity (30).
107 Our hypothesis is that the sweet taste transduction pathway and the taste gustducin G-
108 protein are altered in metabolic diseases contributing to a defective sugar detection,
109 inappropriate plasma enterohormone concentrations and reduced incretin effect.
110 Taking advantage of an RNA sequencing previously performed in human EECs, we
111 examined the relationship between obesity and T2D and the *GNAT3* expression in these
112 cells. We studied the expression of *Gnat3* and other genes involved in sweet taste

transduction pathway during the onset of metabolic diseases in mouse models fed for 1 to 12 weeks, either on control, high-fat (HFD) or high-fat and high-fructose (HFD-HF) diets as well as in metabolic improvement induced by an entero-gastro anastomosis (EGA) mouse model (40). Furthermore, to investigate the role of gut microbiota on α-gustducin expression, we performed fecal microbiota transfer.

MATERIAL AND METHODS:

Human study

This study is ancillary to a previously published studies (30) that included subjects with severe obesity involved in a bariatric surgery program (RYGB) carried out at the Pitié-Salpétrière University Hospital, Nutrition and visceral Surgery Departments (Paris, France). Obese subjects were stratified according to their metabolic status, and two groups were constituted: obese subjects without T2D (Ob, n= 14) and obese subjects with T2D (ObD, n= 13) receiving antidiabetic treatments or yet untreated (30). Results related to EEC preparation, RNA-sequencing and its subsequent analysis have been already published (30). The RNA-Seq gene expression data and raw fastq files are available on the GEO repository (www.ncbi.nlm.nih.gov/geo/) under accession number GSE132831.

Animals and diets

Six- and 3-week-old C57BL/6j male mice were obtained from Janvier Labs (France). For the EGA surgical procedure, 7-week-old C57BL/6j male mice were obtained from Charles River Laboratories (France). Mice were housed in groups and maintained on a 12-hour light-dark cycle with *ad libitum* access to water and diet: chow diet (CD: 5% Kcal fat - reference A03-10, Safe-Diets) or high fat diet (60% Kcal fat - D12492, Research Diets) with (HFD-HF) or without (HFD) 30% fructose (Sigma) in drinking water. Food and bedding were irradiated at 10 kGy. Experimental procedures agreed with the French ethical guidelines for animal

studies and were approved by the Regional Animal Care and Use Ethic Committee Charles Darwin C2EA – 05, agreement number (#17401).

EGA surgical procedure

The EGA surgical procedure was performed as previously described (40). In brief, HFD mice undergoing surgery were fasted for 6 h and anaesthetized with 2% isoflurane (Abbott) and air/oxygen. Analgesia was delivered intraperitoneally 30 min before surgery (Buprenorphine, 0.03 mg/kg, Axience SAS) and at the end of the procedure (Ketoprofen, Merial, 1%, diluted 1/100, 200 µL per mouse). Antibioprophylaxy was delivered sub-cutaneous at beginning of the surgery (ceftriaxone 100 mg/kg, Hospira,). The procedure consisted of a pyloric sphincter ligature, followed by an entero-gastric anastomosis connecting the distal jejunum to the stomach, excluding the duodenum and the proximal jejunum from the alimentary tract. Sham-operated mice (simple laparotomy) underwent the same duration of anaesthesia as EGA-operated mice. In both groups, the laparotomy was repaired in two layers. All mice were maintained on a standardized post-operative protocol to monitor pain, body weight and hydration, subcutaneous injection of saline serum and additional analgesia was given as necessary. The mice had access to water and high fat diet right after surgery. Experimental procedures were agreed with the French ethical guidelines for animal studies and approved by the Regional Animal Care and Use Ethic Committee Charles Darwin C2EA – 05, agreement number (#2762).

Fecal microbiota transfer

Mice undergoing 12 weeks of CD and HFD-HF diets were used as fecal microbiota donors. In the morning, feces from the donor mice were collected in sterile containers and immediately diluted in sterile, anoxic Ringer buffer containing 1 g/L L-cysteine as a reducing agent. An aliquot of inoculum was snap frozen in liquid nitrogen and stored at −80◦C for subsequent bacterial composition analysis.

167 Colonization was achieved by intragastric gavage with 200 µL of inoculum once per day for 3
168 consecutive days as described previously (21). 3-week old mice received by gavage with
169 inoculum of CD microbiota (MRCD) or HFD-HF microbiota (MRHFD-HF) and were kept on
170 HFD-HF diet. Gloves were changed between the handling of each group, and all instruments
171 and working area were disinfected with hydrogen peroxide 3% vol/vol.
172
173 **Microbiome composition analysis**
174 Feces from donor mice after 12 weeks of diet, as well as those from recipient mice 3 and 12
175 weeks after microbiota transfer and the inoculum solution were frozen in liquid nitrogen and
176 stored at -80°C upon usage.
177 Detailed pipeline information was previously described in (22) with modifications described in
178 (1). Briefly, fecal DNA was extracted using the PureLink™ Microbiome DNA Purification Kit
179 (Invitrogen) according to the manufacturer's instructions. Bacterial DNA from these samples
180 was sequenced using the minION nanopore DNA sequencing from Oxford Nanopore
181 Technologies (ONT). DNA libraries were prepared using the Ligation Sequencing Kit 109
182 (SQK-LSK 109, ONT), with multiplexing (EXP-NBD104, ONT), so that up to 12 samples
183 could be sequenced at the same time on the same R9 flow-cell. After sequencing, raw fast5
184 read files generated by the MinKNOW™ software (ONT) were base called and demultiplexed
185 using Guppy (version 2.1.3). Taxonomic binning was performed as follow: sequences were
186 then mapped on an 8,000 reference genomes database using Centrifuge and the
187 assignment was further quality-checked using Minimap2. From this step, species-level
188 abundance tables were built and integrated with taxonomic information and sample metadata
189 in phyloseq objects for subsequent analyses with phyloseq R package. Samples were
190 rarified to 35,000 reads per sample before quantitative analyses. All analyses on abundance
191 data were performed after rarefaction and exclusion of rare taxa (detected in less than 20%
192 of the samples). Relative abundances values were calculated for each sample by dividing the
193 rarefied abundances by the sum of the abundances.

194

195 **Body composition**

196 Mouse body composition was measured in vigil mice using the Bruker Minispec mq10 NMR
197 (Bruker Optics) after 3 and 12 weeks of diet, 3 and 12 weeks after microbiota transfer, 1
198 week before the EGA surgery and at day 28 after the EGA surgery. Animals were placed in a
199 clear plastic cylinder (50 mm in diameter) lowered into the device for the duration of the scan
200 (<2 min).

201

202 **Plasma parameter measurements**

203 Blood was withdrawn from the tail vein using EDTA as the anticoagulant. Blood glucose
204 levels were evaluated using a glucometer (Accuchek performa®, Roche). Plasma
205 triglycerides were measured using Triglycerides FS kit from Diasys (Diagnostic Systems).
206 Plasma insulin was determined by Elisa (Alpco, Eurobio). For active GLP-1 determination,
207 blood was collected into EDTA coated Microvettes (SARSTEDT) preloaded with Dipeptidyl
208 peptidase-4 inhibitor (Merck, Millipore). Blood was immediately centrifuged at 4 °C to
209 separate the plasma from the whole blood and stored at -20°C until analysis. Plasma insulin,
210 glucagon, C-peptide, PYY, active GLP-1, GIP and Leptin concentrations were assessed by
211 MILLIPLEX assays (MMHE-44 K Milliplex, EMD Millipore).

212

213 **Glucose and insulin tolerance tests**

214 All experiments were performed on conscious mice. A glucose tolerance test (2g/kg body
215 weight) was performed on mice fasted overnight for 14-16 h (diet and microbiota transfer
216 experiments) or fasted for 6 hours (EGA experiment). For the insulin tolerance test, animals
217 fasted for 6 hours were injected intraperitoneally with 0.5 or 1 unit of insulin/kg body weight
218 (Novorapid®, Novo-Nordisk). For both tests, blood glucose was measured at the tail vein with
219 an AccuCheck Performa glucometer (Roche Diagnostics) at indicated times.

220

221 **Intestinal tissue collection**

Human epithelial cells from obese patient jejunum were collected as described in our previous study (30). Mice undergoing CD, HFD or HFD-HF were euthanized by cervical dislocation, the jejunum was dissected and the mucosa was scrapped to collect epithelial cells before FACS procedure.

EGA-operated and sham-operated mice were anesthetized and decapitated 4 weeks after surgery. Duodenum, proximal and distal jejunum and ileum were frozen in liquid nitrogen and stored at -80°C. Total RNA was extracted using Rneasy mini kit (Qiagen).

Mice undergoing fecal microbiota transfer (FMT) were euthanized by cervical dislocation. The jejunum was turned over and cut before dissociating the epithelium in a cell recovery solution (corning). Total RNA was extracted using Tri-reagent® (Molecular Research Center. Inc.).

FACS for enriched-EEC preparation in mouse

We adapted to mice the FACS method for enriched-EEC preparation in humans described in (30). Epithelial cells were scrapped and rinsed in FACS buffer (PBS, 3% FCS, 2 mM EDTA), blocked with Fc Receptor Binding Inhibitor Antibody (eBioscience) and stained with the following antibodies: CD45-BV421 (Bio Legend), CD326-APC (Biolegend) and CD24-FITC (Biolegend). Dead cells were excluded with propidium iodure (eBiosciences). During sorting experiments, cells were placed in FACS buffer with RNAse inhibitor (Life Technologies). CD24 marker was used to select enteroendocrine, Paneth and stem differentiated cells, CD45 to get rid of B lymphocytes that also expressed CD24 and CD326-APC to select epithelial cells. CD45-negative, CD326 positive, CD24-positive EEC enriched cell fraction was on a jet-in-air flow cytometer, the MoFlo Astrios with Summit software (Beckman Coulter).

Gene expression analysis

In CD45+, CD24- and CD24+ sorted mouse cells, gene expression was measured using QuantiGene™ Plex assay kit (QGP-150-M20021104, ThermoFisher). HPRT, PPIB, PGK1

and RPS18 were used for normalization (41). Relative quantification was determined by the median fluorescent intensity.

Otherwise, reverse transcription using M-MLV reverse transcriptase (Promega) and quantitative PCR with SybrGreen were performed. Gene expression was normalized with RPLP0 expression in mice and cyclophilin expression in humans to obtain relative quantification using the $2^{-\Delta\Delta Ct}$ method. All primers are presented in Table 1.

Statistical analysis

We used GraphPad Prism and R softwares for all statistical analysis. For human data, details of all analyses and tests are described in Osinski & al (30). Briefly, to assess differential expression on semi-quantitative techniques such as RNAseq data, EdgeR (Biocomputing) package was used using negative binomial test. P-values were adjusted using the false discovery rate (FDR) method with a threshold of 0.001. Only genes with count per million (cpm) over 100 for at least 2 individuals were considered. Statistical differences in mice were demonstrated with one-way or two-way ANOVA or t-tests as described in each figure legend after the outliers have been removed with ROUT method (Q=1%) and the sample distribution normality checked with D'Agostino & Pearson omnibus or Shapiro-Wilk tests. For intestinal microbiota analyses, statistics on principal coordinates were computed by permanova with 1000 permutations using adonis function (VEGAN R package) and statistics on cliff-delta were calculated with Wilcoxon-Mann-Whitney analysis using EFFSIZE R package. $p<0.05$ was considered as statistically significance.

RESULTS

Severe obesity and T2D are associated with reduced sweet taste transduction pathway gene expression in human EEC.

The RNA-sequencing transcriptome of jejunal sorted EEC from severely obese patients with (ObD) or without T2D (Ob) has been reported in Osinski & al (30). Here, we analyzed the gene expression of sweet taste transduction pathway, namely *TAS1R3*, *GNAT3*, *PLCB2*,

278 *ITPR3*, *SCN2A*, *TRPM5, CACNA1A*, *SLC2A2* and *SLC2A5* (Fig. 1*A*). We showed that
279 *GNAT3* gene expression was decreased 3-fold (fdr≤0.0001) in ObD patients compared to Ob
280 patients whereas *ITPR3* was increased 2-fold (fdr≤0.0001) (Fig. 1*A*). Furthermore, we
281 showed a strong correlation between *GNAT3* gene expression analysis by RNA-sequencing
282 and by RT-qPCR in Ob and ObD patients (Fig. 1*B*), confirming the down-regulation of
283 GNAT3 by T2D in obesity.
284 This prompted us to explore the regulation of sweet taste transduction pathway genes in
285 animal models with metabolic degradation and after metabolic improvement**.**
286
287 **High-fat high-fructose diet induces more severe metabolic deterioration compared to**
288 **high-fat diet.**
289 To induce different severity of metabolic disorders, mice were fed either with control (CD),
290 high-fat (HFD) or high-fat and high-fructose (HFD-HF) diets for 1 to 12 weeks. Both HFD and
291 HFD-HF prompted a similar weight gain (Fig. 2*A*) compared to CD. Body composition
292 analyses showed an increased lean mass after 12 weeks regardless of the diets (Fig. 2*B*).
293 As expected, increased fat mass was exacerbated after HFD and HFD-HF compared to CD
294 from 3 weeks of diets (Fig. 2*C*) whereas plasma triglycerides were increased after 3 and 12
295 weeks of HFD (Fig. 2*D*). Glucose homeostasis was then analyzed. The area under the curve
296 (AUC) of glycaemia during oral glucose tolerance test (OGTT) revealed glucose intolerance
297 as early as 3 weeks of HFD and HFD-HF diets and the glucose intolerance was accentuated
298 after 12 weeks of HFD-HF (Fig. 2*E* to *G*). After 12 weeks of diets, fasted glycaemia was
299 significantly higher in HFD and in HFD-HF than in CD mice (Fig. 2*H*). Mice fed 12 weeks with
300 HFD-HF displayed higher basal insulin level (Fig. 2*I*), insulin resistance in accordance with
301 elevated HOMA-IR (Fig. 2*J*) and deteriorated insulin tolerance test (Fig. 2*K* and *L*). Together,
302 these results showed that metabolic phenotype of HFD fed mice is characterized by obesity,
303 glucose intolerance and basal hyperglycemia. HFD-HF fed mice displayed a more severe
304 metabolic deterioration. Indeed, HFD-HF fed mice also displayed basal hyperinsulinemia and
305 insulin resistance.

The expression of sweet taste transduction genes is altered in sorted EEC from mice with metabolic deterioration

EEC are rare and scattered along the crypt-villus axis. Therefore, to enable the study of sweet taste pathway gene expression in EEC, a mouse epithelial cell preparation, enriched in EEC, was adapted from our previous work in humans (30) (Fig. 3*A*). Since the mucosa is more difficult to separate from the muscle tissue in mice, we added the CD326 marker to select the epithelial cells (18). CD24 was initially used in mice to separate stem cells that weakly express CD24 from Paneth cells and EEC that strongly express this antigenic marker (42). As shown in Figure 3, *B* to *E*, our cell sorting strategy in mice was validated. Indeed, gene expression of EEC specific markers, namely *ChgA*, *Gip*, *Pyy* and *Pcsk1* and specific markers of Paneth cells and stem cells, *Lyz* and *Lgr5* respectively, were specifically expressed in the CD24+ cell fraction (Fig. 3*F* and *G*). The *ApoA4* gene expression, an enterocyte marker, was significantly higher in the CD24- cell fraction than in the CD24+ cell fraction (Fig. 3*H*). However, an *ApoA4* gene expression in the CD24+ cell fraction showed either a contamination or an unexpected gene expression. More strikingly, the *Gnat3* gene expression was specific of CD24+ cell fraction, indicating that α-gustducin subunit, encoded by this gene, is specific of EEC (Fig. 3*I*).

We examined the expression of sweet taste transduction pathway genes (Fig. 4*A*), namely: the sweet taste receptor (*Tas1r2* and *Tas1r3*), the α gustducin subunit (*Gnat3*), the inositol trisphosphate receptor (*Itpr3*), the phospholipase C β2 (*Plcb2*), the calcium voltage-gated channel subunit alpha 1a (*Cacna1a*), the sodium voltage-gated channel alpha subunit 2 (*Scn2A*) and the transient receptor potential cation channel subfamily M member 5 (*Trpm5*). We also analyzed *Slc2a2* and *Slc2a5* gene expression, which encode respectively for GLUT2 and GLUT5, two sugar transporters (Fig. 4*B*). The expression of *Tas1r2* and *Tas1r3* were not detectable. We noticed that *Gnat3* expression in EEC was decreased after 3 weeks of HFD and HFD-HF as well as after 12 weeks of HFD (Fig. 4*A, top*). Moreover, we observed

a decrease in *Itpr3* and *Trpm5* gene expression in EEC after 12 weeks of HFD (Fig. 4*A, bottom*) and an increased *Slc2a5* gene expression after 3 weeks of HFD-HF (Fig. 4*B, top*). *Gnat3* gene expression seems to be highly responsive to high fat diets resulting in a marked reduction in expression levels in EEC. Interestingly, at 3 weeks of HFD and HFD-HF diets, *Gnat3 (p=0.014), Plcb2 (p=0.019)* and *Trpm5 (p=0.019)* gene expression was negatively correlated with body weight of mice (*data not shown*). We concluded that expression of genes involved in sweet taste transduction pathway in EEC was altered by obesity, glucose intolerance, and basal hyperglycemia.

The α-gustducin gene expression is partly rescued by surgery-induced hyperglycemia remission in mice

To evaluate if the altered sweet taste transduction pathway gene expression within EEC could be corrected after weight loss and diabetes remission, we used EGA surgery in mice (a surrogate of the RYGB in humans), as described before (2, 40). EGA surgery forms a loop that excludes the duodenum and proximal jejunum from alimentary tract. After surgery, the food contained in the stomach is then discharged directly into the distal jejunum which becomes the first segment in contact with the nutrients (Fig. 5*A*). EGA surgery was performed in obese mice fed 8 weeks on HFD. After surgery, the HFD was maintained for additional 4 weeks in sham- (control mice) and EGA-operated mice and metabolic parameters and gene expression were evaluated. In agreement with previous experiments (40) in sham-operated mice, body weight recovered 30 days after surgery whereas a long-term decreased body weight was observed in EGA-operated mice during the follow-up (Fig. 5*B*). Body composition analyses confirmed a stable lean mass in both sham-operated and EGA-operated mice whereas fat mass decreased in EGA-operated mice after surgery (Fig. 5*C* and *D*) as well as plasma leptin level (Table 2). The AUC of glycemia during an OGTT were significantly lower in EGA-operated than in sham-operated mice as well as fasted basal glycemia (Fig. 5 *E* to *H*). The improvement of glucose tolerance in EGA-operated mice resulted from a decrease in insulin (Fig. 5*I*) and C-peptide secretions (Table 2). Glucagon

levels were similarly reduced during OGTT in all groups during glucose challenge (Table 2). Insulin sensitivity was improved in EGA-operated mice since plasma insulin levels and HOMA-IR were decreased (Fig. 5*I* to *K*). Thus, gut anatomy modifications performed with EGA surgery allowed to induce body weight loss, and improvement of basal glycemia, glucose tolerance, insulin secretion and insulin sensitivity. The gut anatomy modifications were concomitant with an increased glucose-induced GLP-1 secretion and elevated basal PYY level (Fig.5 *L* and *M*). In contrast, glucose-induced GIP secretion was decreased in EGA-operated compared to sham-operated mice (Fig. 5*N*).

Gnat3 expression was determined in duodenum, proximal and distal jejuna, and ileum in sham- and EGA-operated mice. *Gnat3* expression in sham-operated increased in distal jejunum and ileum compared to duodenum segment (Fig. 6*A*). In EGA-operated, *Gnat3* expression increased in proximal jejunum compared to duodenum segment (Fig. 6*A*).

We therefore compared the intestinal segments which are the first to receive the alimentary bolus, i.e. the duodenum of sham with the distal jejunum of EGA-operated (Fig. 6*B*). After metabolic improvement, *Gnat3* expression was increased 3-fold in the distal jejunum of EGA-operated mice compared to the duodenum of sham-operated mice (Fig. 6*B*). Concerning the second intestinal segment receiving alimentary bolus, i.e. proximal jejunum of sham- and ileum of EGA- operated mice no statistical difference was observed (Fig. 6*C*). These results show that the EGA surgery in mice restores *Gnat3* expression in the new first alimentary tract of the gut which subsequently could contribute to improve the glucose-induced GLP-1 secretion.

A diet-induced dysbiotic intestinal microbiota does not directly modify the intestinal *Gnat3* expression

In order to determine if changes in the expression of sweet taste α G protein in the gut are dependent of microbiota composition, we performed fecal microbiota transfer (FMT) from donor mice fed 12 weeks with HFD-HF diet or CD to young recipient mice at weaning and then fed for additional 3 or 12 weeks with a HFD-HF (Fig. 7*A*). We chose to transfer the fecal

389 microbiota at weaning period when the gut microbiota is not well established in recipient
390 mice, to facilitate the transferred microbiota implantation (21). The fecal microbiota and the
391 inoculum of donor mice either fed CD or fed HFD-HF were sequenced and analyzed.
392 Principal coordinate analysis based on Bray-Curtis β-diversity matrix revealed that, the
393 overall bacterial composition of microbiota and inoculum of HFD-HF mice were significantly
394 different from microbiota and inoculum of CD mice (Fig. 7*B*). In the CD recipient mice
395 (MRCD) and HFD-HF recipient mice (MRHFD-HF) gut microbiota compositions were also
396 significantly different both 3 and 12 weeks after the FMT, despite an overlap at 3 weeks,
397 indicating overall different gut microbiota profiles which increased throughout the follow-up
398 (Fig. 7*C*).
399 The relative abundance of bacteria genus showed the presence of *Akkermansia* and
400 *Bacteroides* in MRCD at 3 and 12 weeks after transfer (Fig.7D, lanes 3 and 4) but not in
401 MRHFD-HF (Fig. 7D, lanes 7 and 8). Concerning bacteria species, CD inoculum was
402 characterized by a high abundance of *Bacteroides cellulosilyticus* and *Faecalibaculum*
403 *rodentium* while HFD-HF inoculum was characterized by a high abundance of *Lactococcus*
404 *lactis* and *Streptococcus thermophilus* (Fig. 7E). Cliff's δ estimates (CDe) revealed that the
405 MRCD microbiota at both 3 and 12 weeks after transfer was characterized by a major
406 enrichment in *Akkermansia muciniphila (CDe>0.47),* whereas 8 species were highly
407 represented in MRHFD-HF at 12 weeks after transfer (Cde<0.47) (Fig. 7*F*). We noticed a
408 high abundance of *Lactococcus lactis* (Fig. 7*E* and *F*) that could be mainly due to a
409 contamination in high-fat diet (6). Furthermore, 12 weeks after FMT, *Faecalibaculum*
410 *rodentium,* characteristic of the CD inoculum, and *Streptococcus thermophilus*, characteristic
411 of the HFD-HF inoculum, were found both in a high abundance in MRCD and in MRHFD-HF,
412 respectively (Fig. 7*F*). We therefore conclude that the fecal microbiota transfer was only
413 partial since the MRCD and MRHFD-HF microbiota are not strictly identic to the respective
414 inoculum.
415 Despite differences in species abundance between MRCD microbiota and MRHFD-HF
416 microbiota, we did not observe differences in body weight gain between MRCD mice and

MRHFD-HF mice (Fig. 8*A*). As expected, the fat mass and lean mass of MRCD mice and MRHFD-HF mice increased between 3 and 12 weeks under HFD-HF but no difference between MRCD mice and MRHFD-HF mice was observed (Fig. 8*B* and *C*). The glucose tolerance measured by the AUC of the OGTT showed that the MRHFD-HF mice presented a statistically significant increased glucose tolerance between 3 and 12 weeks after FMT whereas the MRCD mice did not (Fig. 8*D*), despite a similar increase in basal glycaemia between 3 and 12 weeks (Fig. 8*E*). The gene expression of *Gnat3* in the jejunal epithelial cells in MRCD and MRHFD-HF mice was similar between 3 and 12 weeks after FMT (Fig. 8*F*). However, we observed a tendency to decrease in *Gnat3* gene expression at 3 and 12 weeks after FMT when we compared MRCD mice and HFD-HF mice. These results showed that FMT from HFD-HF mice with metabolic disorders (obesity, glucose intolerance and insulin-resistance) did not directly impact the sweet taste G protein expression in recipient mice.

DISCUSSION

In this study we demonstrate that EEC expression of the sweet taste α-gustducin is reduced in severely obese individuals with T2D. In mice diet-induced obesity, glucose intolerance and basal hyperglycemia, the expression of *Gnat3*, *Itpr3* and *Trpm5* involved in sweet taste transduction pathway were decreased in sorted EEC. Interestingly, the weight loss and the improved glucose homeostasis after EGA in mice led to the restoration of *Gnat3* expression in the new alimentary tract and improved glucose-induced GLP-1 secretion. However, metabolic disorders-induced dysbiotic microbiota did not modify the sweet taste α-gustducin gene expression in mouse intestine. Our data support a role for the sweet taste transduction pathway in mediating GLP-1 secretion in improving glucose homeostasis in mice and this pathway may have therapeutic implications to treat metabolic disease.

EEC are rare, scattered in the intestinal epithelium and difficult to isolate. Recently, the surface marker CD24 was successfully used to enrich EEC from jejunum of obese patients (30). Here, we adapted to mice the EEC sorting method previously described in human (30).

445 *Pcsk1* expression indicated that GLP-1 EECs were present in the CD326+/CD24+ cell
446 fraction. Indeed, *Pcsk1* codes the PC1/3 pro-hormone convertase that cleaves the
447 proglucagon into GLP-1 specifically in intestine. Although we could not exclude having
448 selected a type of EEC, our previous study showed that enriched human EEC fraction
449 displayed no less than 12 enterohormones (30). More strikingly, we showed here that *Gnat3*
450 gene expression is specifically expressed in the EEC cell fraction. The sweet taste
451 transduction pathway was first described at the level of taste buds in the tongue (29, 35).
452 Nevertheless, the existence of this signaling pathway in the EEC was now recognized (24).
453 Indeed, α-gustducin, as well as the β and γ subunits of the gustducin G protein, T1R2-T1R3,
454 PLCβ2, and TRPM5 were expressed in EEC (16). In addition, expression of T1R2, T1R3 and
455 α-gustducin has been described in the murine EEC line STC-1 but not in the enterocyte
456 absorptive cell lines CaCo2-TC7, IEC-6 or FHs74Int (11).
457 Sweet taste thresholds are modified by multiple factors including genetics. Interestingly,
458 polymorphisms of *TAS1R3* and *GNAT3* genes were associated with taste disorder (5). Mice
459 lacking α-gustducin, T1R2 or T1R3 displayed a defective glucose-induced GLP-1 secretion
460 (12, 16, 19). Interestingly, it has been demonstrated that the gene expression of *Tas1r2 and*
461 *Tas1r3* was decreased in the duodenum of diet-induced obesity in mice or in genetically
462 obese *Ob*/*Ob* mice. Moreover, *Trpm5* gene expression was also decreased in diet-induced
463 obese mice (15). Recently, Smith *et al*, suggested that sweet taste receptor has evolved to
464 modulate glucose absorption *via* the regulation of its transport and to prevent the
465 development of exacerbated hyperglycemia due to the ingestion of high levels of sugars (38).
466 Here we analyzed the gene expression of the sweet taste transduction pathway in metabolic
467 diseases in human EEC. We showed that T2D decreased expression of *GNAT3* and
468 increased expression of *ITPR3* in EEC in obese individuals. These results highlighted an
469 altered gene expression involved in the intestinal sweet taste signaling pathway in individuals
470 with metabolic diseases for several years. Our mouse models exposed to either HFD or
471 HFD-HF diets allowed us to analyze the sweet taste transduction pathway during the

472 metabolic disorder onset with severity degrees. In EEC the impaired *Gnat3* expression
473 occurred in the early stages of obesity as early as 3 weeks of HFD or HFD-HF diet, whereas
474 decreased *Trpm5* and *Itrpr3* expression occurred after 12 weeks of diets. We concluded that
475 in EEC the sweet taste transduction pathway, at least at the level of gene expression, was
476 altered by obesity, glucose intolerance, and basal hyperglycemia. This gene expression
477 alteration was aggravated with the metabolic disorder duration. However, additional basal
478 hyperinsulinemia and insulin resistance contributing to a more severe metabolic phenotype
479 did not aggravate the alteration of the sweet taste transduction pathway. Moreover, the
480 down-regulation of *Gnat3* was similar regardless the high-fat diet, with or without fructose. It
481 has been previously described an alteration of the sweet taste transduction pathway in
482 duodenum of high-fat diet-induced obese mice or of genetically *Ob*/*Ob* mice (15). Together,
483 those results suggested that obesity impairs the sweet taste transduction pathway, at least at
484 gene expression level.
485 We previously showed that obesity itself did not impact the GLP-1+, CCK+, GIP+ and PYY+
486 cell density in obese patients when compared to non-obese patients (30). But rather T2D
487 was associated to a decreased GLP-1+ cell density and an impaired lineage in human
488 obesity (30). Thus, in our mouse models of diet-induced obesity and insulin resistance, we
489 could hypothesize that the EEC density was not decreased and did not contribute to *Gnat3*
490 down-regulation, although without excluding it.
491 Bariatric surgery is associated with metabolic improvement, a rapid remission of T2D and a
492 restoration of gut hormone release, particularly of GLP-1 (17, 37). In mice, EGA results in
493 weight loss, improved glucose tolerance and increased GLP-1 secretion in response to
494 glucose (40). Here, we reported an over-expression of *Gnat3* in the most proximal segments
495 of the intestine after EGA surgery. In this context, we compared the *Gnat3* expression in the
496 duodenum of sham-operated mice to the distal jejunum of EGA-operated mice and the
497 proximal jejunum of sham-operated to the ileum of EGA-operated mice because these
498 segments were the first in contact with the flow of nutrients after surgical intestinal

remodeling. The increased expression of *Gnat3* in the lower small intestine could contribute to the improving of GLP-1 secretion in response to glucose.

Metabolic diseases leading to dysbiosis of the intestinal microbiota (31), we hypothesized that dysbiotic microbiota from diet-induced obese mice would cause intestinal alteration of gene expression involved in sweet taste pathway. Our results showed that the HFD-HF FMT to recipient mice kept on HFD-HF diet (MRHFD-HF) did not impact the weight gain and the basal glycaemia compared to the CD FMT (MRCD). However, we observed a higher aggravation of glucose intolerance in MRHFD-HF mice than in MRCD. This could be due to the presence of *Akkermansia muciniphila* in MRCD mice which is absent in MRHFD-HF mice. Indeed, *Akkermansia municiphila* is usually associated with a healthy metabolic status (8). However, the FMT induced only a trending decrease in *Gnat3* gene expression in MRHFD-HF mice. However, it could not be ruled out that the microbiota of the host fed HFD-HF masked the effect of HFD-HF FMT on *Gnat3* intestinal expression. Thus, we could not conclude if intestinal microbiota impacted or not the sweet taste transduction pathway.

In conclusion, our data highlighted: 1/ the sweet taste transduction pathway in EECs plays an important role for glucose homeostasis, at least at gene expression level; 2/ metabolic disorders led to altered gene expression of sweet taste signaling pathway in intestine contributing to impaired GLP-1 secretion; 3/ after surgical intestinal modifications increased expression of α-gustducin contributed to metabolic improvement.

We speculated that targeting the sweet taste transduction pathway in intestine, and in particular sweet taste receptors, could ameliorate the endogenous secretion of GLP-1 in individuals with obesity and T2D.

Acknowledgements. The authors thank F. Deknuydt for EEC sorting (CytoICANplatform, ICAN) and A. Lacombe for EGA surgery procedure (PreClinICAN platform, ICAN).

Author Contributions. LLG, CR, CO, AR, PS, FA conceived and designed experiments; LLG, CR, CO, PB, CA performed experiments; LLG, CR, CO, EP, JD, FA, PS, AR, HAS

analyzed data; LLG, FA, AR, PS, KC interpreted results of experiments; LLG prepared figures; LLG, AR, PS drafted manuscript; LLG, AR, PS, KC, FA edited and revised manuscript; AR, PS approved final version of manuscript.

Fundings. This work was supported by INSERM, Sorbonne University, MSDAvenir, LLG and JD received a doctoral fellowship from Sorbonne University. This work was supported by the Fondation pour la Recherche Médicale, grant number FDT202001010875 to LLG.

Competing Interests. No potential conflict of interest relevant to this article were reported

References

1. **Alili R**, **Belda E**, **Clément K**, **Le P**, **Prifti E**, **Zucker J-D**, **Wirth T**. Exploring Quantitative Metagenomics Studies using Oxford Nanopore Sequencing: A Computational and Experimental Protocol. Research Square [https://doi.org/10.21203/rs.3.rs-131495/v1].

2. **Amouyal C**, **Castel J**, **Guay C**, **Lacombe A**, **Denom J**, **Migrenne-Li S**, **Rouault C**, **Marquet F**, **Georgiadou E**, **Stylianides T**, **Luquet S**, **Le Stunff H**, **Scharfmann R**, **Clément K**, **Rutter GA**, **Taboureau O**, **Magnan C**, **Regazzi R**, **Andreelli F**. A surrogate of Roux-en-Y gastric bypass (the enterogastro anastomosis surgery) regulates multiple beta-cell pathways during resolution of diabetes in ob/ob mice. *EBioMedicine* 58, 2020. doi: 10.1016/j.ebiom.2020.102895.

3. **Aranias T**, **Grosfeld A**, **Poitou C**, **Omar AA**, **Le Gall M**, **Miquel S**, **Garbin K**, **Ribeiro A**, **Bouillot J-L**, **Bado A**, **Brot-Laroche E**, **Clément K**, **Leturque A**, **Guilmeau S**, **Serradas P**. Lipid-rich diet enhances L-cell density in obese subjects and in mice through improved L-cell differentiation. *J Nutr Sci* 4: e22, 2015. doi: 10.1017/jns.2015.11.

4. **Aron-Wisnewsky J**, **Prifti E**, **Belda E**, **Ichou F**, **Kayser BD**, **Dao MC**, **Verger EO**, **Hedjazi L**, **Bouillot J-L**, **Chevallier J-M**, **Pons N**, **Le Chatelier E**, **Levenez F**, **Ehrlich SD**, **Dore J**, **Zucker J-D**, **Clément K**. Major microbiota dysbiosis in severe obesity: fate after bariatric surgery. *Gut* 68: 70–82, 2019. doi: 10.1136/gutjnl-2018-316103.

5. **Bae J-W**, **Kim U-K**, **Kwon T-J**, **Choi S-J**, **Ye M-K**. Polymorphisms of TAS1R3 and GNAT3 Genes Are Associated with Patients with Taste Disorder. *Journal of Life Science* 21: 412–416, 2011. doi: 10.5352/JLS.2011.21.3.412.

6. **Bisanz JE**, **Upadhyay V**, **Turnbaugh JA**, **Ly K**, **Turnbaugh PJ**. Meta-Analysis Reveals Reproducible Gut Microbiome Alterations in Response to a High-Fat Diet. *Cell Host & Microbe* 26: 265-272.e4, 2019. doi: 10.1016/j.chom.2019.06.013.

7. **Borg CM**, **le Roux CW**, **Ghatei MA**, **Bloom SR**, **Patel AG**, **Aylwin SJB**. Progressive rise in gut hormone levels after Roux-en-Y gastric bypass suggests gut adaptation and explains altered satiety. *British Journal of Surgery* 93: 210–215, 2006. doi: 10.1002/bjs.5227.

8. **Dao MC**, **Everard A**, **Aron-Wisnewsky J**, **Sokolovska N**, **Prifti E**, **Verger EO**, **Kayser BD**, **Levenez F**, **Chilloux J**, **Hoyles L**, **Consortium M-O**, **Dumas M-E**, **Rizkalla SW**, **Doré J**, **Cani PD**, **Clément K**. Akkermansia muciniphila and improved metabolic health during a dietary intervention in obesity: relationship with gut microbiome richness and ecology. *Gut* 65: 426–436, 2016. doi: 10.1136/gutjnl-2014-308778.

9. **Debédat J**, **Sokolovska N**, **Coupaye M**, **Panunzi S**, **Chakaroun R**, **Genser L**, **Turenne G de**, **Bouillot J-L**, **Poitou C**, **Oppert J-M**, **Blüher M**, **Stumvoll M**, **Mingrone G**, **Ledoux S**, **Zucker J-D**, **Clément K**, **Aron-Wisnewsky J**. Long-term Relapse of Type 2 Diabetes After Roux-en-Y Gastric Bypass: Prediction and Clinical Relevance. *Diabetes Care* 41: 2086–2095, 2018. doi: 10.2337/dc18-0567.

10. **Depoortere I**. Taste receptors of the gut: emerging roles in health and disease. *Gut* 63: 179–190, 2014. doi: 10.1136/gutjnl-2013-305112.

11. **Dyer J**, **Salmon KSH**, **Zibrik L**, **Shirazi-Beechey SP**. Expression of sweet taste receptors of the T1R family in the intestinal tract and enteroendocrine cells. *Biochemical Society Transactions* 33: 302–305, 2005. doi: 10.1042/BST0330302.

12. **Geraedts MCP**, **Takahashi T**, **Vigues S**, **Markwardt ML**, **Nkobena A**, **Cockerham RE**, **Hajnal A**, **Dotson CD**, **Rizzo MA**, **Munger SD**. Transformation of postingestive glucose responses after deletion of sweet taste receptor subunits or gastric bypass surgery. *American Journal of Physiology-Endocrinology and Metabolism* 303: E464–E474, 2012. doi: 10.1152/ajpendo.00163.2012.

13. **Gerspach AC**, **Steinert RE**, **Schönenberger L**, **Graber-Maier A**, **Beglinger C**. The role of the gut sweet taste receptor in regulating GLP-1, PYY, and CCK release in humans. *American Journal of Physiology-Endocrinology and Metabolism* 301: E317–E325, 2011. doi: 10.1152/ajpendo.00077.2011.

14. **Harvey EJ**, **Arroyo K**, **Korner J**, **Inabnet WB**. Hormone Changes Affecting Energy Homeostasis after Metabolic Surgery. *Mount Sinai Journal of Medicine: A Journal of Translational and Personalized Medicine* 77: 446–465, 2010. doi: https://doi.org/10.1002/msj.20203.

15. **Herrera Moro Chao D**, **Argmann C**, **Van Eijk M**, **Boot RG**, **Ottenhoff R**, **Van Roomen C**, **Foppen E**, **Siljee JE**, **Unmehopa UA**, **Kalsbeek A**, **Aerts JMFG**. Impact of obesity on taste receptor expression in extra-oral tissues: emphasis on hypothalamus and brainstem. *Sci Rep* 6, 2016. doi: 10.1038/srep29094.

16. **Jang H-J**, **Kokrashvili Z**, **Theodorakis MJ**, **Carlson OD**, **Kim B-J**, **Zhou J**, **Kim HH**, **Xu X**, **Chan SL**, **Juhaszova M**, **Bernier M**, **Mosinger B**, **Margolskee RF**, **Egan JM**. Gut-expressed gustducin and taste receptors regulate secretion of glucagon-like peptide-1. *PNAS* 104: 15069–15074, 2007. doi: 10.1073/pnas.0706890104.

17. **Jirapinyo P**, **Jin DX**, **Qazi T**, **Mishra N**, **Thompson CC**. A Meta-Analysis of GLP-1 After Roux-En-Y Gastric Bypass: Impact of Surgical Technique and Measurement Strategy. *OBES SURG* 28: 615–626, 2018. doi: 10.1007/s11695-017-2913-1.

18. **Kawasaki H**, **Yoshida T**, **Horiguchi K**, **Ohama T**, **Sato K**. Characterization of anoikis-resistant cells in mouse colonic epithelium. *J Vet Med Sci* 75: 1173–1180, 2013. doi: 10.1292/jvms.13-0005.

19. **Kokrashvili Z**, **Mosinger B**, **Margolskee RF**. T1r3 and α-Gustducin in Gut Regulate Secretion of Glucagon-like Peptide-1. *Annals of the New York Academy of Sciences* 1170: 91–94, 2009. doi: https://doi.org/10.1111/j.1749-6632.2009.04485.x.

20. **Larraufie P**, **Roberts GP**, **McGavigan AK**, **Kay RG**, **Li J**, **Leiter A**, **Melvin A**, **Biggs EK**, **Ravn P**, **Davy K**, **Hornigold DC**, **Yeo GSH**, **Hardwick RH**, **Reimann F**, **Gribble FM**. Important Role of the GLP-1 Axis for Glucose Homeostasis after Bariatric Surgery. *Cell Rep* 26: 1399-1408.e6, 2019. doi: 10.1016/j.celrep.2019.01.047.

21. **Le Roy T**, **Debédat J**, **Marquet F**, **Da-Cunha C**, **Ichou F**, **Guerre-Millo M**, **Kapel N**, **Aron-Wisnewsky J**, **Clément K**. Comparative Evaluation of Microbiota Engraftment Following Fecal Microbiota Transfer in Mice Models: Age, Kinetic and Microbial Status Matter. *Front Microbiol* 9, 2019. doi: 10.3389/fmicb.2018.03289.

22. **Lu H**, **Giordano F**, **Ning Z**. Oxford Nanopore MinION Sequencing and Genome Assembly. *Genomics Proteomics Bioinformatics* 14: 265–279, 2016. doi: 10.1016/j.gpb.2016.05.004.

23. **Madsbad S**, **Holst JJ**. GLP-1 as a Mediator in the Remission of Type 2 Diabetes After Gastric Bypass and Sleeve Gastrectomy Surgery. *Diabetes* 63: 3172–3174, 2014. doi: 10.2337/db14-0935.

24. **Margolskee RF**, **Dyer J**, **Kokrashvili Z**, **Salmon KSH**, **Ilegems E**, **Daly K**, **Maillet EL**, **Ninomiya Y**, **Mosinger B**, **Shirazi-Beechey SP**. T1R3 and gustducin in gut sense sugars to regulate expression of Na+-glucose cotransporter 1. *PNAS* 104: 15075–15080, 2007. doi: 10.1073/pnas.0706678104.

25. **Meier JJ**, **Nauck MA**. Incretins and the development of type 2 diabetes. *Curr Diab Rep* 6: 194–201, 2006. doi: 10.1007/s11892-006-0034-7.

26. **Mingrone G**, **Panunzi S**, **De Gaetano A**, **Guidone C**, **Iaconelli A**, **Capristo E**, **Chamseddine G**, **Bornstein SR**, **Rubino F**. Metabolic surgery versus conventional medical therapy in patients with type 2 diabetes: 10-year follow-up of an open-label, single-centre, randomised controlled trial. *Lancet* 397: 293–304, 2021. doi: 10.1016/S0140-6736(20)32649-0.

27. **Miras AD**, **Kamocka A**, **Pérez-Pevida B**, **Purkayastha S**, **Moorthy K**, **Patel A**, **Chahal H**, **Frost G**, **Bassett P**, **Castagnetto-Gissey L**, **Coppin L**, **Jackson N**, **Umpleby AM**, **Bloom SR**, **Tan T**, **Ahmed AR**, **Rubino F**. The Effect of Standard Versus Longer Intestinal Bypass on GLP-1 Regulation and Glucose Metabolism in Patients With Type 2 Diabetes Undergoing Roux-en-Y Gastric Bypass: The Long-Limb Study. *Diabetes Care*. Ahead of print, 2020 doi: 10.2337/dc20-0762

28. **Nauck M**, **Stöckmann F**, **Ebert R**, **Creutzfeldt W**. Reduced incretin effect in Type 2 (non-insulin-dependent) diabetes. *Diabetologia* 29: 46–52, 1986. doi: 10.1007/BF02427280.

29. **Nelson G**, **Hoon MA**, **Chandrashekar J**, **Zhang Y**, **Ryba NJP**, **Zuker CS**. Mammalian Sweet Taste Receptors. *Cell* 106: 381–390, 2001. doi: 10.1016/S0092-8674(01)00451-2.

30. **Osinski C**, **Le Gléau L**, **Poitou C**, **de Toro-Martin J**, **Genser L**, **Fradet M**, **Soula HA**, **Leturque A**, **Blugeon C**, **Jourdren L**, **Hubert EL**, **Clément K**, **Serradas P**, **Ribeiro A**. Type 2 diabetes is associated with impaired jejunal enteroendocrine GLP-1 cell lineage

in human obesity. *Int J Obes (Lond)* 45: 170–183, 2021. doi: 10.1038/s41366-020-00694-1.

31. **Pascale A**, **Marchesi N**, **Marelli C**, **Coppola A**, **Luzi L**, **Govoni S**, **Giustina A**, **Gazzaruso C**. Microbiota and metabolic diseases. *Endocrine* 61: 357–371, 2018. doi: 10.1007/s12020-018-1605-5.

32. **Paternoster S**, **Falasca M**. Dissecting the Physiology and Pathophysiology of Glucagon-Like Peptide-1. *Front Endocrinol* 9, 2018. doi: 10.3389/fendo.2018.00584.

33. **Peterli R**, **Steinert RE**, **Woelnerhanssen B**, **Peters T**, **Christoffel-Courtin C**, **Gass M**, **Kern B**, **von Fluee M**, **Beglinger C**. Metabolic and Hormonal Changes After Laparoscopic Roux-en-Y Gastric Bypass and Sleeve Gastrectomy: a Randomized, Prospective Trial. *OBES SURG* 22: 740–748, 2012. doi: 10.1007/s11695-012-0622-3.

34. **Ren X**, **Zhou L**, **Terwilliger R**, **Newton S**, **De Araujo IE**. Sweet taste signaling functions as a hypothalamic glucose sensor. *Front Integr Neurosci* 3, 2009. doi: 10.3389/neuro.07.012.2009.

35. **Roper SD**. Taste buds as peripheral chemosensory processors. *Seminars in Cell & Developmental Biology* 24: 71–79, 2013. doi: 10.1016/j.semcdb.2012.12.002.

36. **Rozengurt N**, **Wu SV**, **Chen MC**, **Huang C**, **Sternini C**, **Rozengurt E**. Colocalization of the α-subunit of gustducin with PYY and GLP-1 in L cells of human colon. *American Journal of Physiology-Gastrointestinal and Liver Physiology* 291: G792–G802, 2006. doi: 10.1152/ajpgi.00074.2006.

37. **Sjöström L**. Review of the key results from the Swedish Obese Subjects (SOS) trial – a prospective controlled intervention study of bariatric surgery. *Journal of Internal Medicine* 273: 219–234, 2013. doi: https://doi.org/10.1111/joim.12012.

38. **Smith K**, **Karimian Azari E**, **LaMoia TE**, **Hussain T**, **Vargova V**, **Karolyi K**, **Veldhuis PP**, **Arnoletti JP**, **de la Fuente SG**, **Pratley RE**, **Osborne TF**, **Kyriazis GA**. T1R2 receptor-mediated glucose sensing in the upper intestine potentiates glucose absorption through activation of local regulatory pathways. *Molecular Metabolism* 17: 98–111, 2018. doi: 10.1016/j.molmet.2018.08.009.

39. **Steinert RE**, **Gerspach AC**, **Gutmann H**, **Asarian L**, **Drewe J**, **Beglinger C**. The functional involvement of gut-expressed sweet taste receptors in glucose-stimulated secretion of glucagon-like peptide-1 (GLP-1) and peptide YY (PYY). *Clinical Nutrition* 30: 524–532, 2011. doi: 10.1016/j.clnu.2011.01.007.

40. **Troy S**, **Soty M**, **Ribeiro L**, **Laval L**, **Migrenne S**, **Fioramonti X**, **Pillot B**, **Fauveau V**, **Aubert R**, **Viollet B**, **Foretz M**, **Leclerc J**, **Duchampt A**, **Zitoun C**, **Thorens B**, **Magnan C**, **Mithieux G**, **Andreelli F**. Intestinal Gluconeogenesis Is a Key Factor for Early Metabolic Changes after Gastric Bypass but Not after Gastric Lap-Band in Mice. *Cell Metabolism* 8: 201–211, 2008. doi: 10.1016/j.cmet.2008.08.008.

41. **Verbist B**, **Adriaensen E**, **Keersmaekers V**, **Putri D**, **Crabbe M**, **Derks M**, **Bagdziunas R**, **Laenen G**, **De Wolf H**. Analyzing magnetic bead QuantiGene® Plex 2.0 gene expression data in high throughput mode using QGprofiler. *BMC Bioinformatics* 20: 378, 2019. doi: 10.1186/s12859-019-2975-2.

42. **Wong VWY**, **Stange DE**, **Page ME**, **Buczacki S**, **Wabik A**, **Itami S**, **van de Wetering M**, **Poulsom R**, **Wright NA**, **Trotter MWB**, **Watt FM**, **Winton DJ**, **Clevers H**, **Jensen**

KB. Lrig1 controls intestinal stem-cell homeostasis by negative regulation of ErbB signalling. *Nat Cell Biol* 14: 401–408, 2012. doi: 10.1038/ncb2464.

43. **Young LA**, **Buse JB**. GLP-1 receptor agonists and basal insulin in type 2 diabetes. *Lancet* 384: 2180–2181, 2014. doi: 10.1016/S0140-6736(14)61409-4.

44. **Young RL**. Sensing via Intestinal Sweet Taste Pathways. *Front Neurosci* 5, 2011. doi: 10.3389/fnins.2011.00023.

700 Table 1. *RT-qPCR primer sequences*

	Gene	Forward primer	Reverse primer
Murine primers	*Rplp0*	AATCAGCCAGAAGGTCCAAA	CGCAAATGCAGATGGATC
	Gnat3	AATCAGCCAGAAGGTCCAAA	TTTCCCAGATTCACCTGCTC
Human primers	*Cyclophillin*	GCCTTAGCTACAGGAGAGAA	TTTCCTCCTGTGCCATCTC
	GNAT3	AGCGAGATGCAAGAACCGTA	CATTCTTATGGATGATCTTCATTTGT

701

702

Table 2. *Plasma hormone concentrations during OGTT in sham- and EGA-operated mice.*

[pg/mL]	Time (min)	0	15	30	60
C-peptide	sham	1 763 ± 203	3 382 ± 436 ***	2 282 ± 276	1 459 ± 151
	EGA	669 ± 74$^{\#}$	1 969 ± 285 *$^{\#\#}$	721 ± 90$^{\#\#\#}$	565 ± 94 $^{\#}$
Glucagon	sham	26 ± 4	37 ± 6	30 ± 4	22 ± 4
	EGA	38 ± 4$^{\#}$	39 ± 3	44 ± 9	42 ± 5$^{\#}$
Leptin	sham	17 870 ± 8 791	16 129 ± 5 614	13 258 ± 2 979	11 856 ± 3 064
	EGA	757 ± 229$^{\#}$	786 ± 359$^{\#}$	1069 ± 405$^{\#}$	705 ± 238$^{\#}$

EGA surgery was performed in obese mice fed 8 weeks on HFD. After surgery, the HFD was maintained for an additional 4 weeks in sham-operated (control mice) and EGA-operated mice. OGTT was performed at 0, 15, 30 and 60 minutes after glucose gavage in sham (n= 14) and EGA (n=13) mice. Statistical differences were calculated with a two way ANOVA and Post hoc Tukey's multiple comparisons tests. *: $p<0.05$, **: $p<0.01$ compared to 0 min for each group. $^{\#}$: $p<0.05$, $^{\#\#}$: $p<0.01$, $^{\#\#\#}$: $p<0.001$ in EGA-operated mice compared to sham-operated mice at the same time point.

FIGURE LEGENDS

Fig. 1. Sweet taste gene expression in human EEC from obese patients with or without T2D. A: Expression of genes involved in sweet taste transduction and glucose transporters in EEC from jejunum of obese individuals with (ObD, n=13) or without type 2 diabetes (Ob, n=14): *TAS1R3*, *GNAT3*, *PLCB2*, *ITPR3*, *SCN2A, TRPM5 and CACNA1A*, which code for taste receptor type 1 member 3, α-gustducin subunit, phospholipase C β2, inositol trisphosphate receptor, sodium voltage-gated channel alpha subunit 2, transient receptor potential cation channel subfamily member 5, calcium voltage-gated channel subunit alpha 1A respectively, and *SLC2A2* and *SLC2A5* which code for GLUT2 and GLUT5, respectively. Data are presented as means ± SEM. B: Correlation of GNAT3 expression by RT-qPCR and RNAseq in human EEC of Ob (n=11) and ObD (n=11) subjects. Statistical significance was calculated with (A) unpaired t-test and (B) simple linear regression test (Pearson). *: $p < 0.05$, **: $p < 0.01$ and ****: $p < 0.0001$

Fig. 2. Diet-induced metabolic disorders in mice. A: Body weight is measured weekly for each group of mice fed with diets: CD (black, n=75), HFD (light grey, n=15) and HFD-HF (dark grey, n=75). B: The lean mass and C: The fat mass determined after 3 and 12 weeks of CD (n=10), HFD (n=10) and HFD-HF (n=10) diet by nuclear magnetic resonance. D: Fasting plasma triglycerides of mice fed 3 or 12 weeks with CD (n=13), HFD (n=5), HFD-HF (n=13). Curves of OGTT after 3 weeks (E) and 12 weeks (F) of diets. G: Area under the curve (AUC) during OGTT. H: Fasting blood glucose and I: Fasting plasma insulin before OGTT. J: Homeostasis Assessment of insulin resistance (HOMA-IR). OGTT was performed after fasting overnight with 2g/kg of glucose on mice fed 3 weeks with CD (n=20), HFD (n=10) and HFD-HF (n=20) and on mice fed 12 weeks with CD (n=18), HFD (n=10) and HFD-HF (n=18). K: Insulin tolerance test (ITT) after 12 weeks of diets. L: Decrease of glycemia during the 10 first minutes of ITT. ITT was performed after 6h fasting with 1U/kg of insulin on mice fed 12 weeks with CD (n=10), HFD (n=10) and HFD-HF (n=10). Data are presented as means ±

SEM. Statistical significance was calculated with (A) two-way ANOVA test (R software), (B to E; H to J; and L) one-way ANOVA and post-hoc Tukey's multiple comparisons tests, (F, G, K) two-way ANOVA and post-hoc Tukey's multiple comparisons tests. *: p <0.05,**: p< 0.01, ***: p < 0.001 and ****: p<0.0001; §: p <0.05, §§: p< 0.01, §§§: p < 0.001 and §§§§: p<0.0001 in comparison CD *versus* HFD

Fig. 3. EEC enrichment cell fraction from mouse jejunum. A: Gating strategy for cell sorting by FACS with Propidium iodide, CD45, CD326 and CD24 markers. Gene expression analysis of Chromogranin A (*Chga*). B: Glucose-dependent insulin releasing polypeptide (*Gip*) C), Peptide tyrosine tyrosine (*Pyy*) (D), Prohormone convertase 1 (*Pcsk1*) (E), Lysozyme (*Lyz*) (F), Leucine-rich repeat-containing G-protein coupled receptor 5 (*Lgr5*) (G), Apolipoprotein A-IV (*Apoa4*) (H) and α-Gustducin (*Gnat3*) (I) in different isolated cell types using Quantigene plex assay. CD45+ cells (white) are mostly composed by immune cells (n=24), CD24- cells (light grey) are mostly composed by enterocytes (n=24) and CD24+ cells (dark grey) are mostly composed by EECs (n=22). Data are presented as means ± SEM. Statistical significance was calculated with one-way ANOVA and post-hoc Tukey's multiple comparisons tests. *: p <0.05 ; **: p< 0.01 ; ***: p < 0.001 and ****: p<0.0001

Fig. 4. Expression of genes involved in sweet taste transduction and in glucose absorption in mouse EEC. A: EEC expression of genes involved in sweet taste transduction: α-gustducin *(Gnat3*), inositol trisphosphate receptor *(Itpr3)*, phospholipase C β2 (*Plcb2)*, calcium voltage-gated channel subunit alpha 1a (*Cacna1a),* sodium voltage-gated channel alpha subunit 2 *(Scn2a),* transient receptor potential cation channel subfamily member 5 *(Trpm5*), in mice fed with CD, HFD or HFD-HF for 3 (top) or 12 weeks (bottom). B: EEC expression of genes encoding for GLUT2 (Slc2a2) and GLUT5 (Slc2a5) in mice fed with CD, HFD or HFD-HF for 3 (top) or 12 weeks (bottom). Gene expression was measured by Quantigene plex assay in EEC from mice (CD n= 4 at 3 weeks and n= 3 at 12 weeks; HFD n=4 at 3 and 12 weeks; and HFD-HF n= 3 at 3 weeks and n= 2 at 12 weeks). Note that each

768 value corresponds to EEC from 2 mice. Data are presented as means ± SEM. Statistical
769 significance was calculated with (A and B top) one-way ANOVA and post-hoc Tukey's
770 multiple comparisons tests, (A and B bottom) unpaired t-test. *: p <0.05 ; **: p< 0.01 ; ***: p <
771 0.001 and ****: p<0.0001
772
773 **Fig. 5. Metabolic improvement 4 weeks after mouse intestinal surgery.** A: EGA surgery
774 schema showing the pyloric sphincter ligature, followed by an entero-gastric anastomosis
775 allowing the exclusion of the duodenum and the proximal jejunum of the alimentary tract.
776 Mice fed with HFD for 8 weeks were operated (sham or EGA) and further maintained 4
777 weeks on HFD before analysis. Arrows indicate the alimentary bolus path. B: Body weight
778 after surgery (EGA or sham) is measured for each group: sham-operated (n=16), EGA-
779 operated (n=14). C: The lean mass and D: The fat mass of mice determined before and 4
780 weeks after sham and EGA surgery by nuclear magnetic resonance (n=15 sham-operated,
781 n=14 EGA-operated). E: Fasting blood glucose before and 4 weeks after sham and EGA
782 surgery. Curves of OGTT before (F) and 4 weeks after (G) surgery. H: Area under the curve
783 (AUC) during OGTT before and 4 weeks after sham and EGA surgery. I: Plasma insulin 4
784 weeks after sham and EGA surgery measured during OGTT. J: Fasting plasma insulin 4
785 weeks after surgery. K: HOMA-IR 4 weeks after surgery. Plasma active GLP-1 (L), PYY (M)
786 and GIP (N) 4 weeks after sham and EGA surgery measured during OGTT. OGTT were
787 performed after 6 hours of fasting with 2g/kg of glucose (n=13 sham-operated, n=14 EGA-
788 operated). Nd means *not detectable* (GLP-1 plasma concentration is under the lower level
789 detected with ELISA *i.e*. < 41pg/mL). Data are presented as means ± SEM. Statistical
790 significance was calculated with (B) two-way ANOVA (R software), (C to H) two-way ANOVA
791 and post-hoc Sidak's multiple comparisons tests, (J, K) an unpaired t-test, (I, L to N) two-
792 way ANOVA and post-hoc Tukey's multiple comparisons tests.* : p <0.05 ; ** : p< 0.01 ; *** :
793 p < 0.001 and ****: p<0.0001 as indicated or *versus* time 0 min (panels I and M); § : p <0.05 ;
794 §§ : p< 0.01 ; §§§ : p < 0.001 and §§§§: p<0.0001 in sham *versus* EGA
795

Fig. 6. *Gnat3* gene expression in gut 4 weeks after mouse intestinal surgery. Mice fed with HFD for 8 weeks were operated (sham or EGA) and further maintained 4 weeks on HFD before analysis. A: *Gnat3* expression has been measured by RT-qPCR in sham- and EGA-operated mice 4 weeks after surgery in four intestinal fragments: (1) duodenum, (2) proximal jejunum, (3) distal jejunum and (4) ileum. B: *Gnat3* expression in the first intestinal segment receiving alimentary bolus in sham- and EGA-operated mice 4 weeks after surgery. C: *Gnat3* expression in the second intestinal segment receiving alimentary bolus in sham- and EGA-operated mice 4 weeks after surgery. n= 16 sham-operated mice and n= 13 EGA-operated mice. Data are presented as means ± SEM. Statistical significance was calculated with (A) one-way ANOVA and post-hoc Tukey's multiple comparisons tests, (B and C) unpaired t-test. *: $p<0.05$, ***: $p<0.001$, ****: $p<0.0001$

Fig. 7. Analysis of mouse fecal microbiota after FMT. A: Experiment design of FMT: 6 weeks old male donor mice are fed 12 weeks with CD or HFD-HF and feces are collected to prepare inoculum. The inoculum is used to transfer the fecal microbiota by gavage in 3 weeks old male recipient mice MRCD or MRHFD-HF. Recipient mice are kept on HFD-HF for 12 weeks. Analyses were made 3 and 12 weeks after FMT. B: Principal coordinate analysis of donor mice fecal microbiota from mice fed CD (n= 4) and HFD-HF (n=2) and inoculum solution composed of pooled feces from CD (n=2) or HFD-HF (n=2) C: Principal coordinate analysis of recipient mice microbiota 3 and 12 weeks after microbiota transfer from CD (n=6 and n=5, respectively) and from HFD-HF (n=6 and n=7, respectively). D: Genus abundance in donor mice, inoculum and recipient mice 3 and 12 weeks after FMT. E: Abundance of *Bacteroides cellulosilyticus, Lactococcus lactis, Faecalibaculum rodentium and Streptococcus thermophilus* in the inoculum from CD and HFD-HF fed mice. Abundance is represented by the reads/rarefaction threshold. F: The magnitude difference of species abundance in recipient mice according to microbiota 3 and 12 weeks after transfer ($p<0.05$). Note that the all species that are statistically different between MRCD and MRHFD-HF mice present a large magnitude effect (Cliff-delta ≥ 0.474).

Fig. 8. Metabolic parameters and intestinal α-Gustducin expression in mice after FMT. A: Body weight is measured weekly for each group of male mice during 12 weeks after FMT in MRCD mice (n= 20) and in MRHFD-HF mice (n=20). B: The lean mass and C: The fat mass of mice determined by nuclear magnetic resonance 3 and 12 weeks after the FMT. MRCD (n=6 and n=5, respectively) and MRHFD-HF (n=6 and n=7, respectively). D: Area under the curve (AUC) during OGTT 3 and 12 weeks after FMT. E: Fasting glycemia before OGTT. OGTT was performed after fasting overnight with 2g/kg of glucose on 5 MRCD mice and 5 MRHFD-HF mice at 3 weeks and 5 MRCD and 5 MRHFD-HF at 12 weeks. F: *Gnat3* gene expression measured in epithelial jejunum of MRCD (n= 4 at 3 and 12 weeks after the FMT) and MRHFD-HF (n=4 at 3 weeks and n= 5 at 12 weeks after the FMT). Data are presented as means ± SEM. Statistical significance was calculated with one-way ANOVA and post-hoc Tukey's multiple comparisons tests. ** : $p< 0.01$; *** : $p < 0.001$ and ****: $p<0.0001$

A

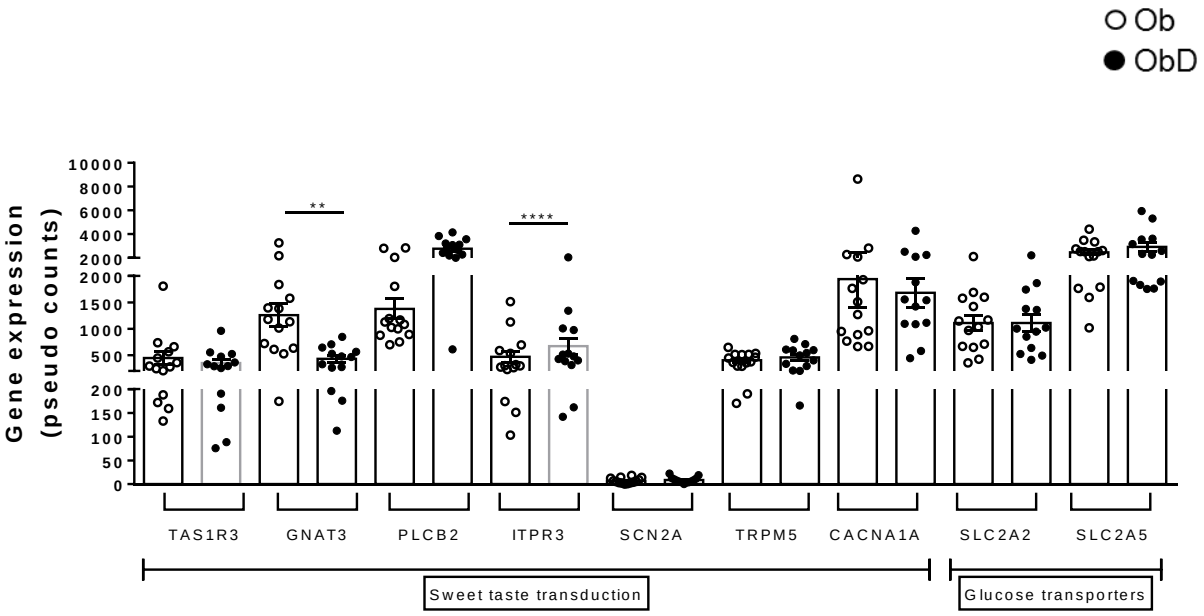

B

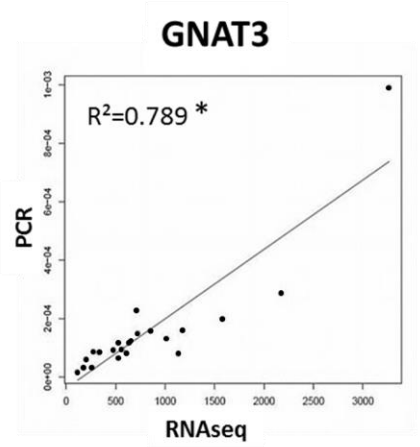

Figure 1, Le Gléau L & al

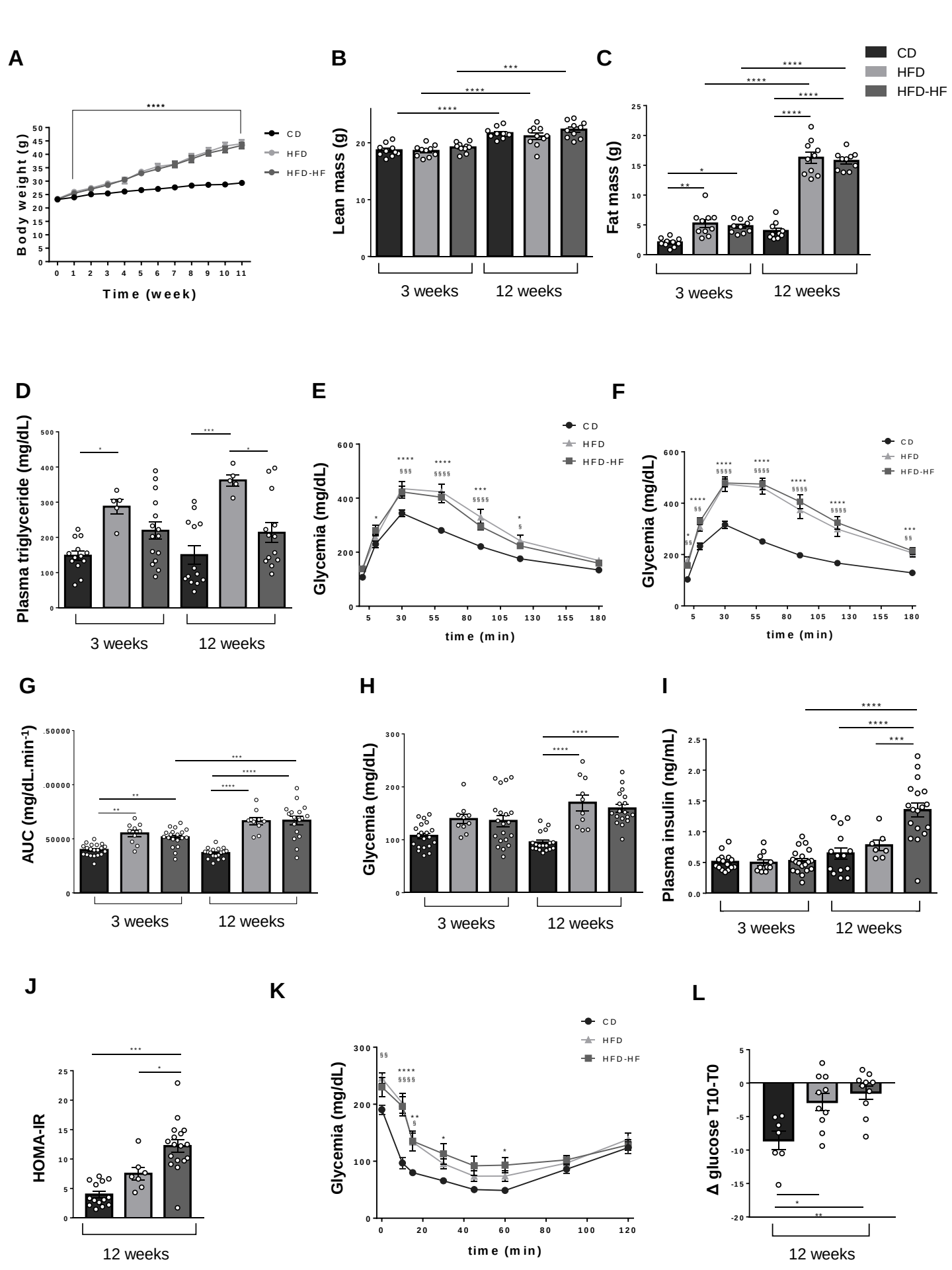

Revised (R2) Figure 2, Le Gléau L & al

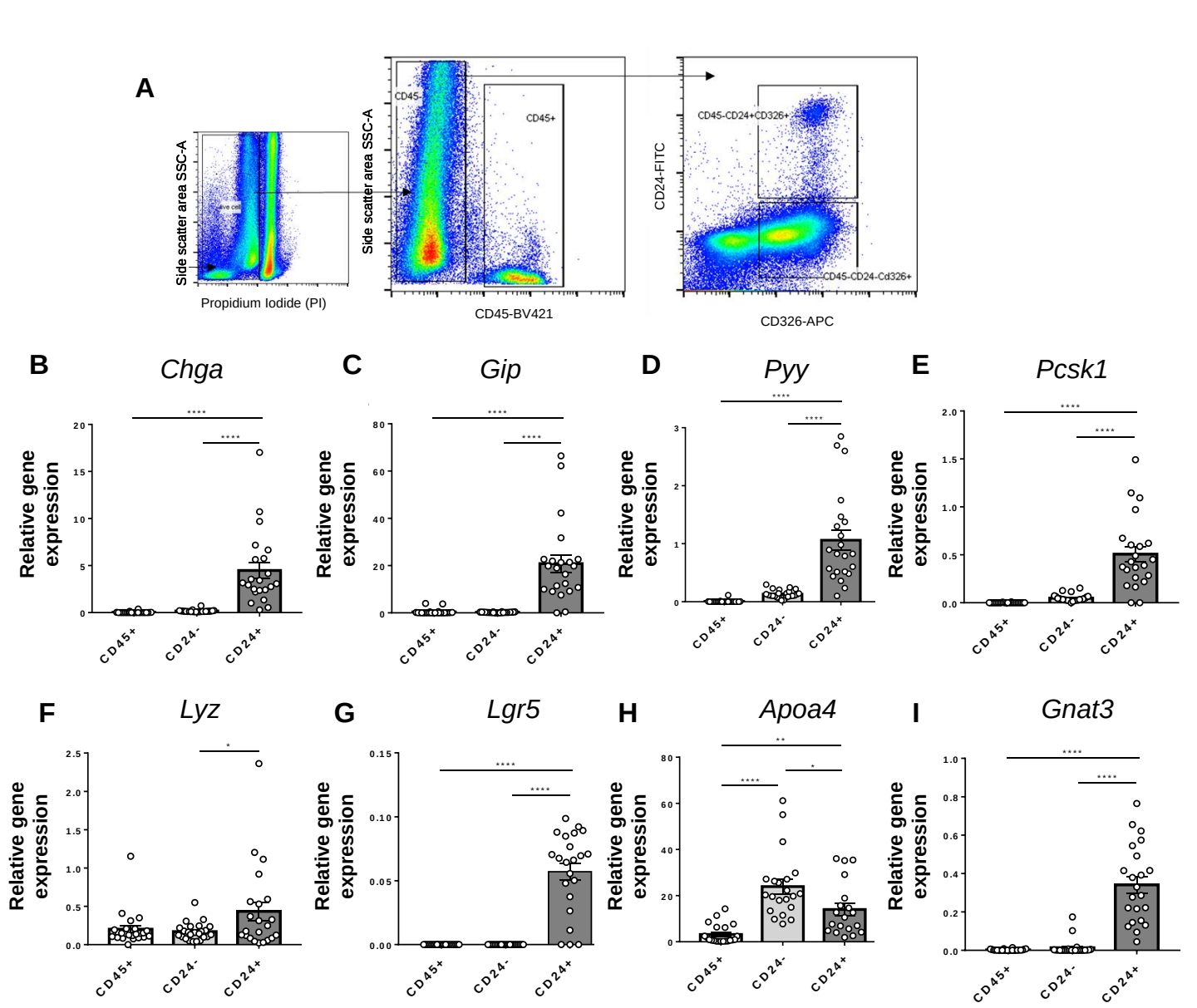

Figure 3, Le Gléau L & al

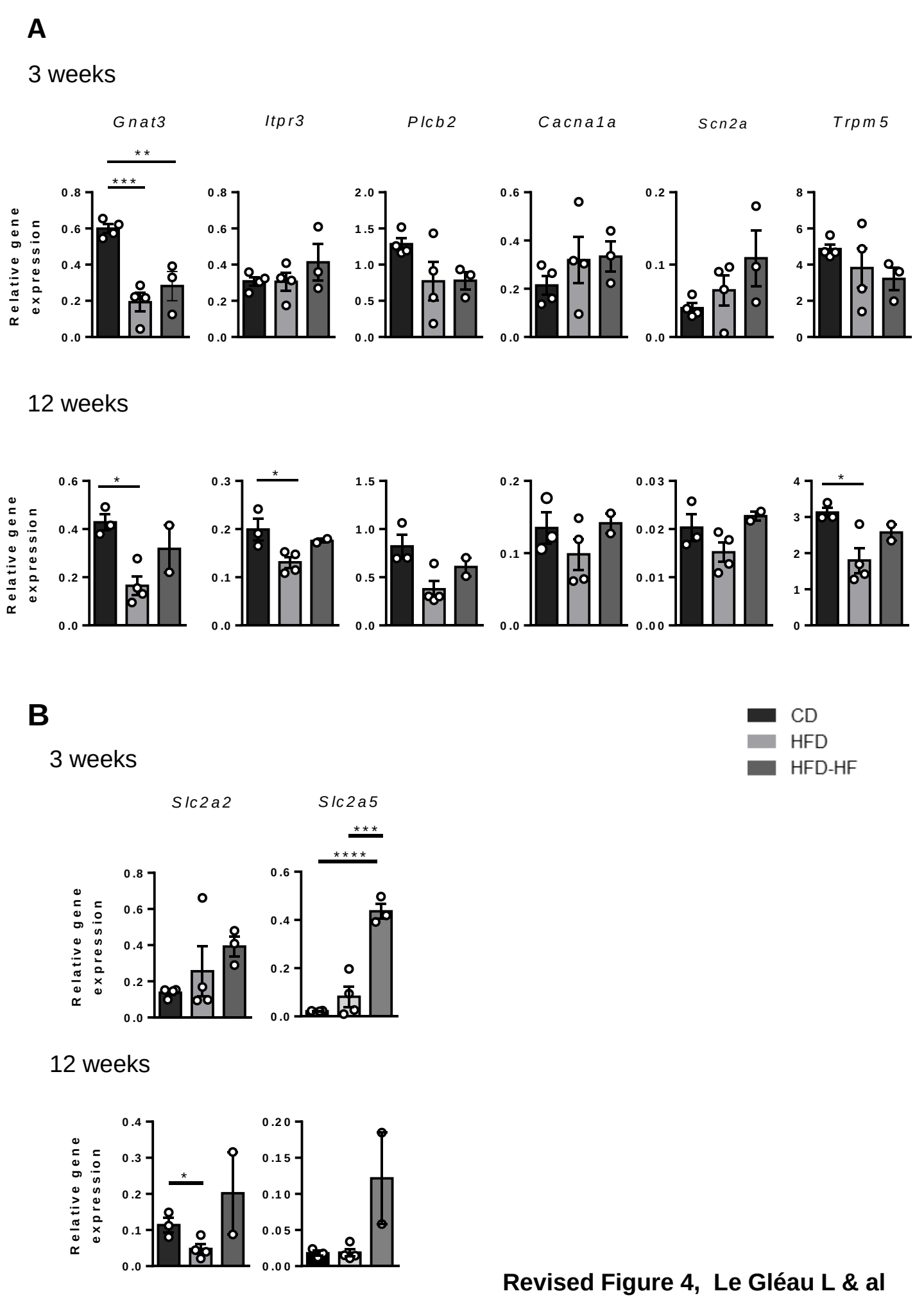

Revised Figure 4, Le Gléau L & al

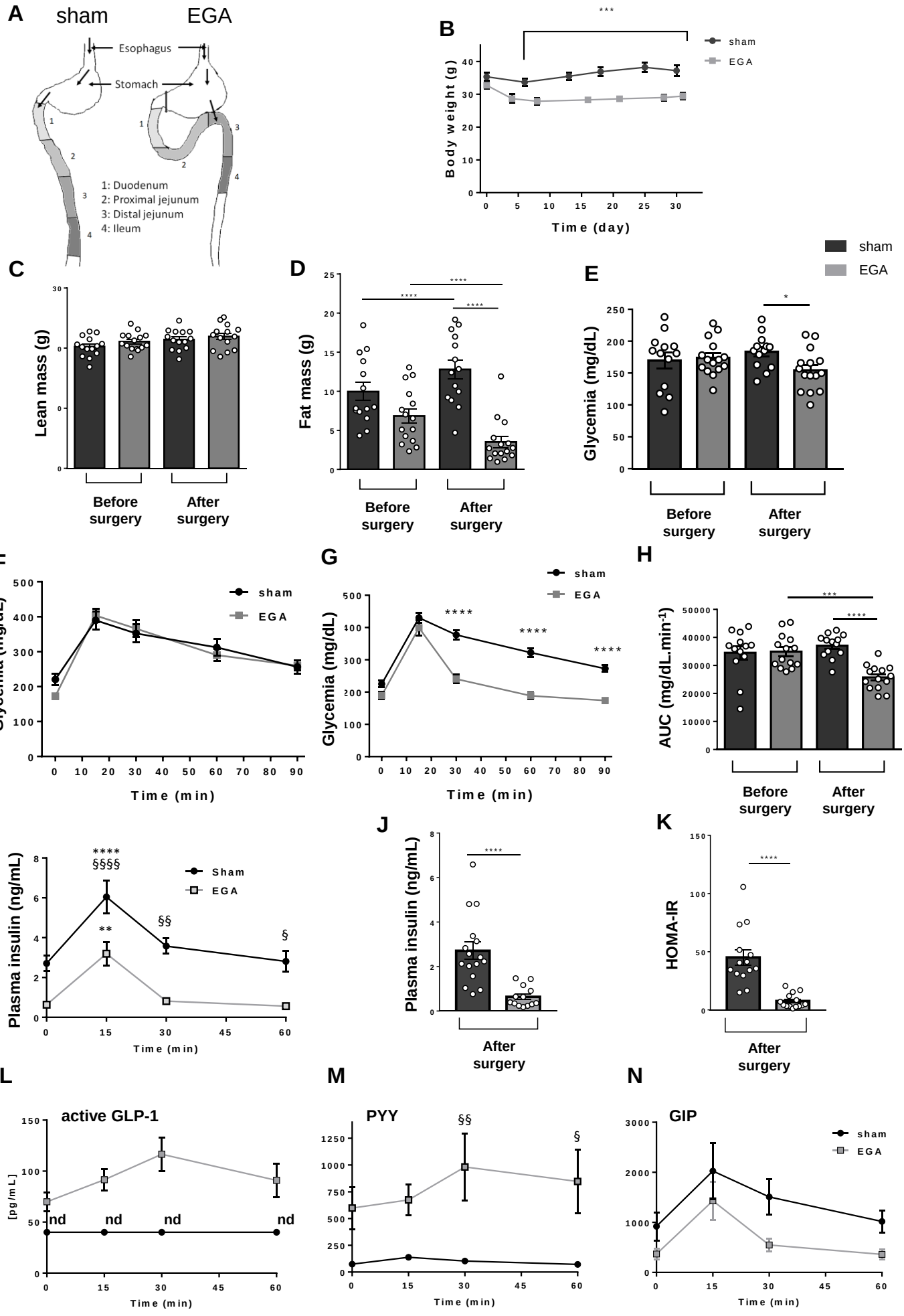

Revised (R2) Figure 5, Le Gléau & al

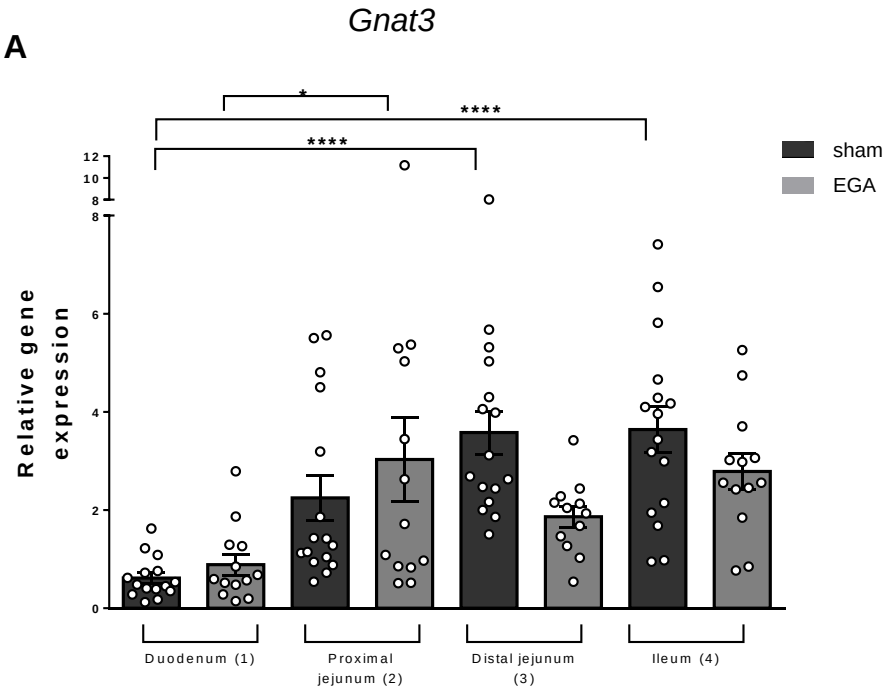

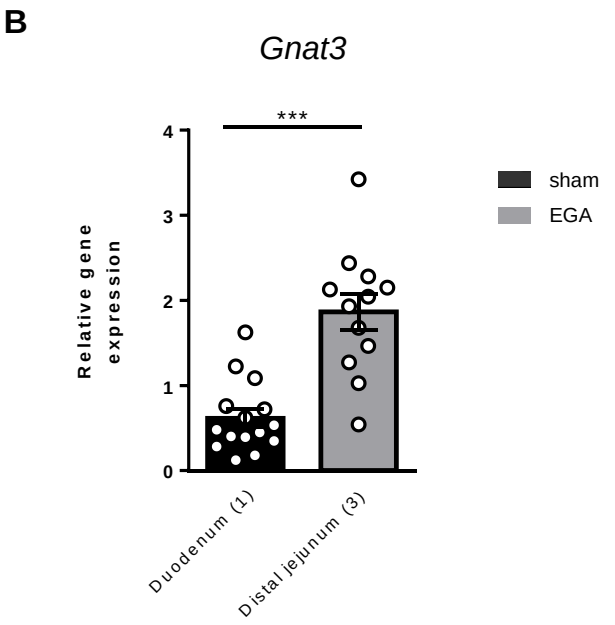

First intestinal segment receiving alimentary bolus

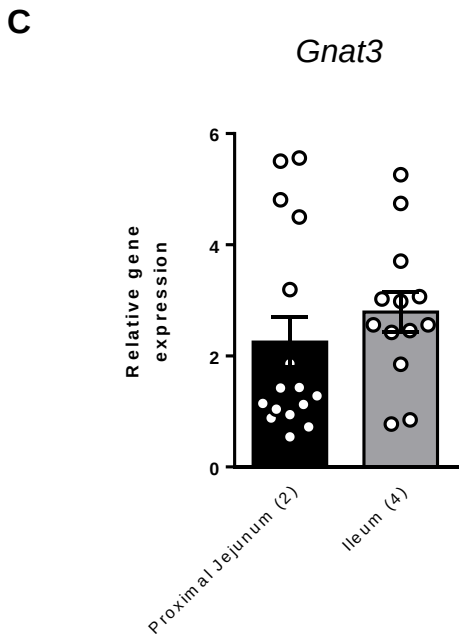

Second intestinal segment receiving alimentary bolus

Revised Figure 6, Le Gléau L & al

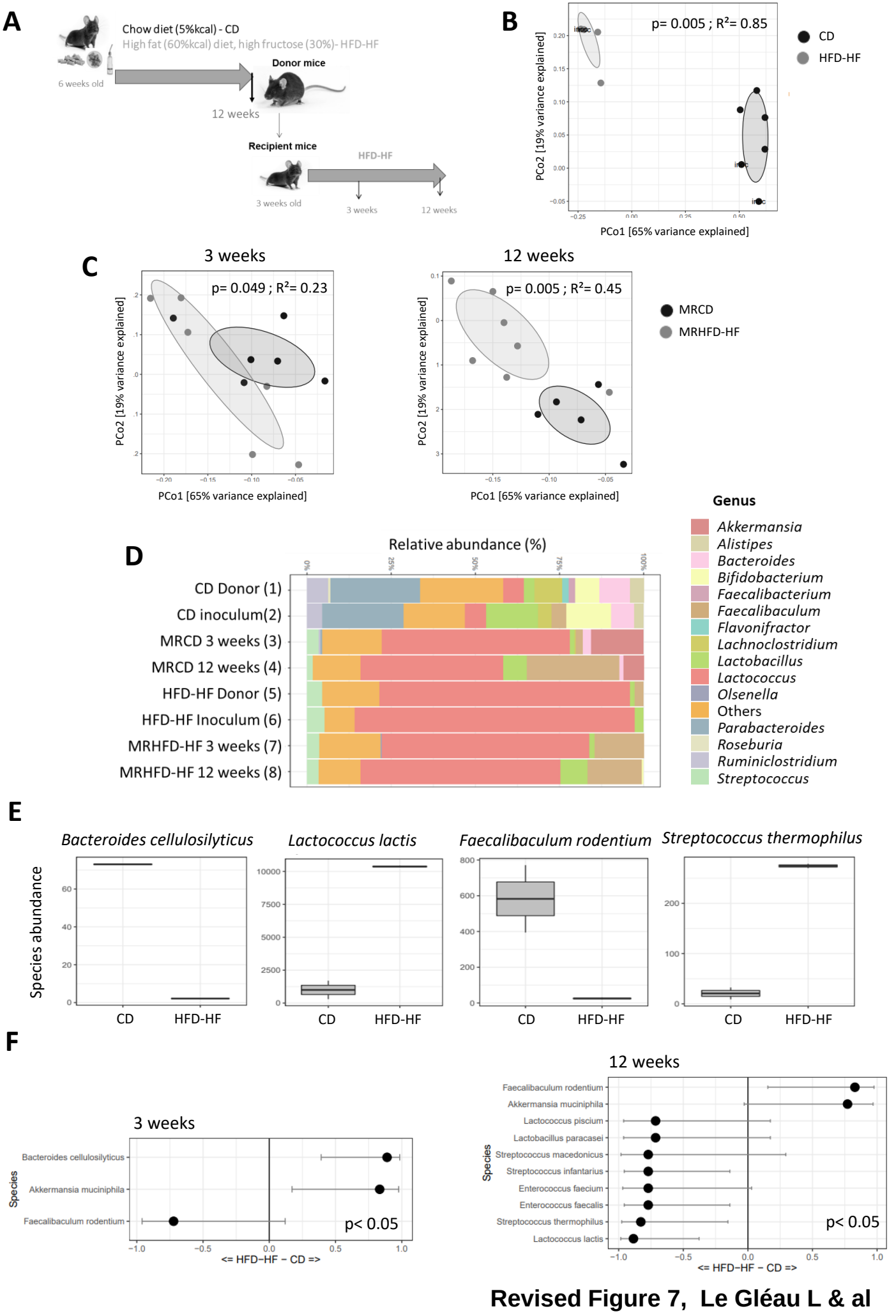

Revised Figure 7, Le Gléau L & al

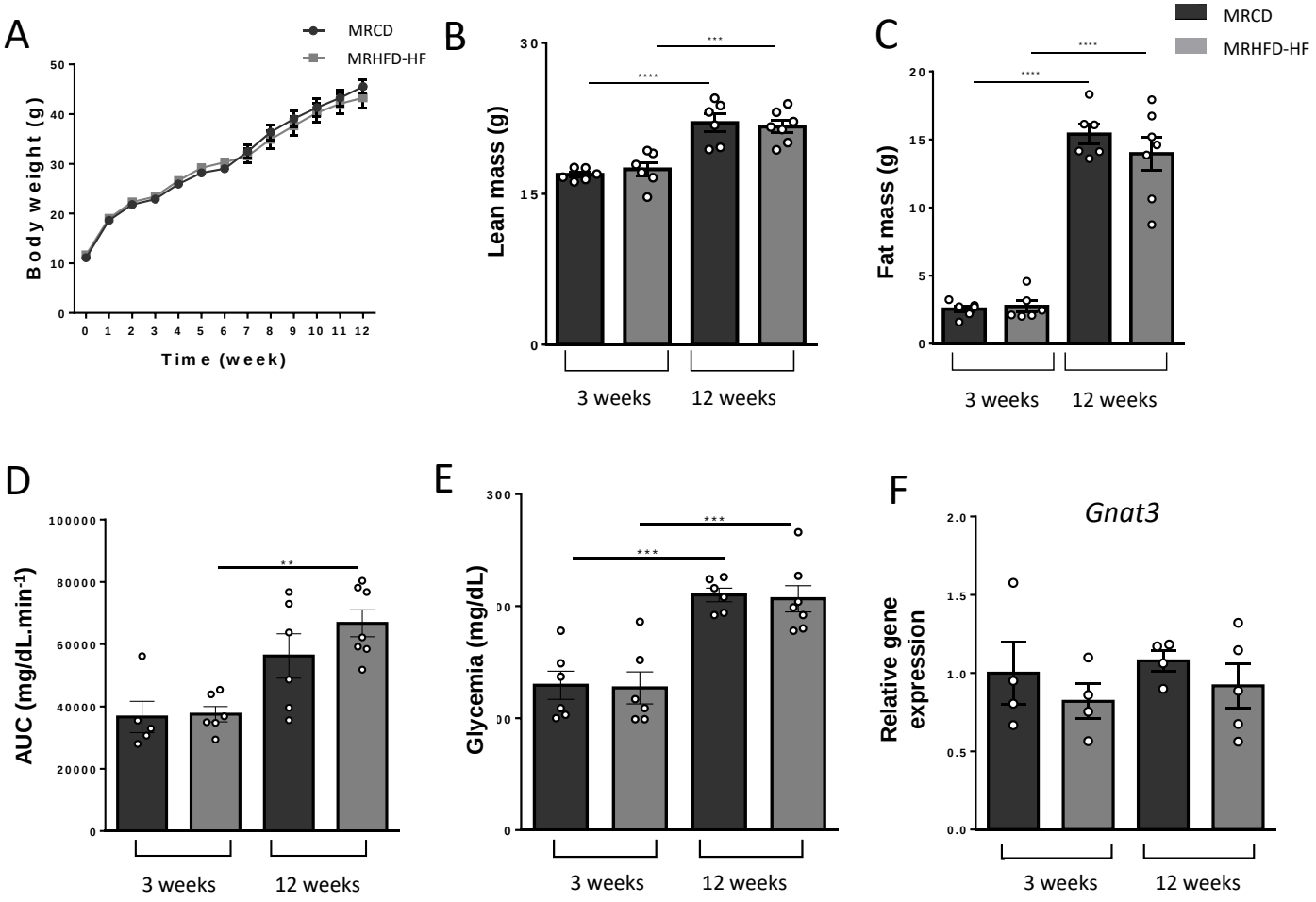

Revised Figure 8, Le Gléau L & al

Intestinal alteration of α-gustducin and sweet taste signaling pathway in metabolic diseases is partly rescued after weight loss and diabetes remission

Methods

1- Sweet taste transduction pathway in human enteroendocrine cells (EEC)

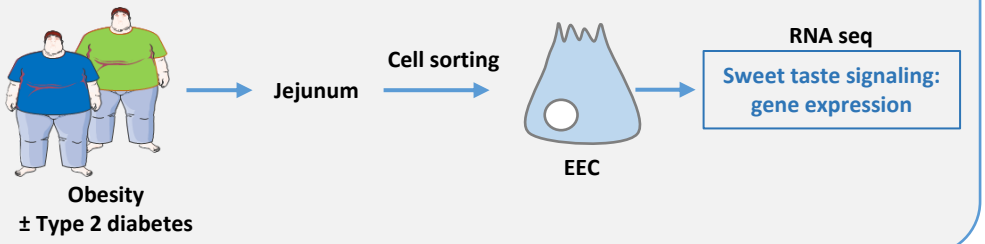

2- Metabolic deterioration in mice fed with high-fat diet (HFD) ± fructose (HFD-HF)

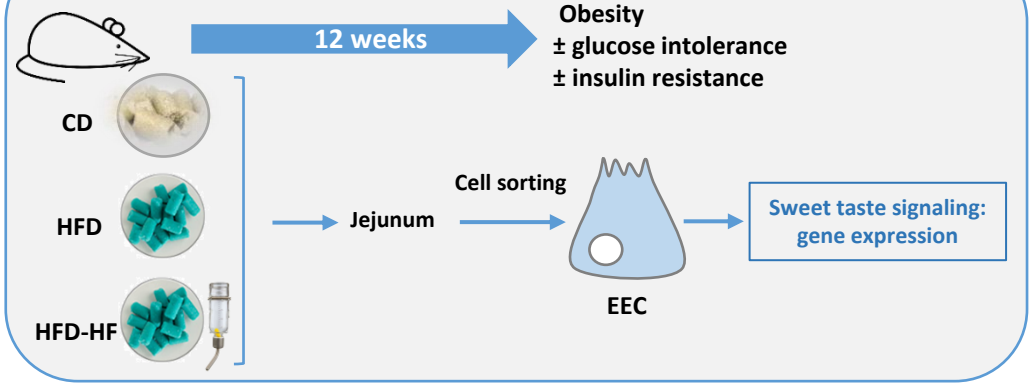

3- Metabolic improvement in mice after Entero-Gastro-Anastomosis (EGA) surgery

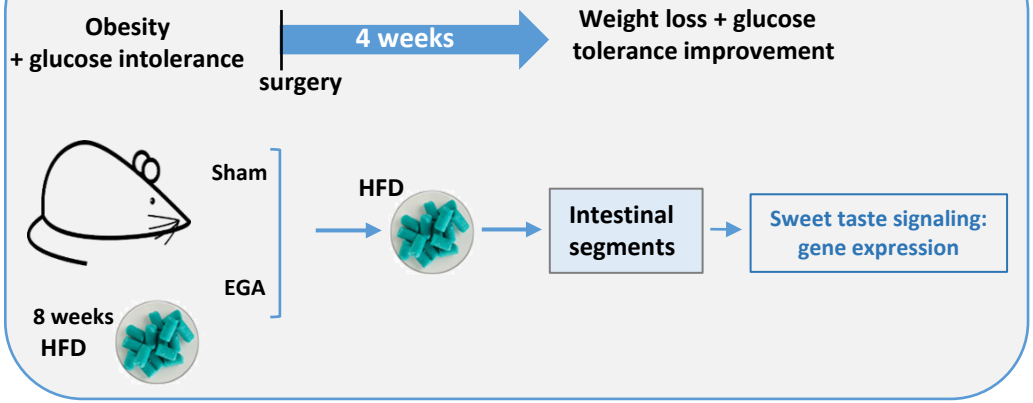

Sweet taste transduction pathway in the GLP-1 enteroendocrine cell in response to carbohydrates

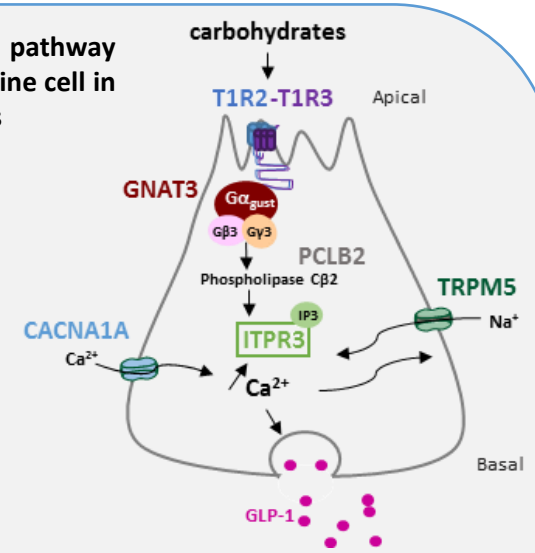

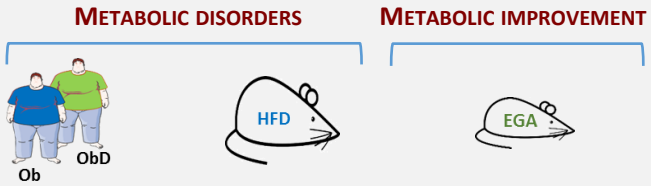

Gene expression

	EEC	EEC	intestine
GNAT3	↘	↘	↘
PCLB2	→	→	nd
ITPR3	↗	↘	nd
CACNA1A	→	→	nd
TRPM5	→	↘	nd

nd: not determinated

CONCLUSIONS: Metabolic diseases are associated with altered gene expression of sweet taste signaling in the intestine. This could contribute to impaired GLP-1 secretion, that is partly rescued after metabolic improvement .